In presenting the dissertation as a partial fulfillment of the requirements for an advanced degree from the Georgia Institute of Technology, I agree that the Library of the Institute shall make it available for inspection and circulation in accordance with its regulations governing materials of this type. I agree that permission to copy from, or to publish from, this dissertation may be granted by the professor under whose direction it was written, or, in his absence, by the Dean of the Graduate Division when such copying or publication is solely for scholarly purposes and does not involve potential financial gain. It is understood that any copying from, or publication of, this dissertation which involves potential financial gain will not be allowed without written permission.

3/17/65
b

AN ALTERNATING CURRENT MAGNETOTHERMOELECTRIC HEAT PUMP

A THESIS

Presented to

The Faculty of the Graduate Division

by

Donald Beatty Wall

In Partial Fulfillment

of the Requirements for the Degree

Doctor of Philosophy

in the School of Mechanical Engineering

Georgia Institute of Technology

December, 1966

AN ALTERNATING CURRENT

MAGNETOTHERMOELECTRIC HEAT PUMP

Approved:

Chairman

Date approved by Chairman: 11/25/67

ACKNOWLEDGMENTS

The author would like to express sincere appreciation to the many people who have encouraged him throughout his life, especially to his mother who first urged him to attend college and to his understanding wife who helped sustain him through graduate school.

The author is very grateful to Dr. Walter O. Carlson, the faculty advisor for this thesis, whose understanding, encouragement, and professional guidance have led to the completion of this work. The constructive comments and the time given by the reading committee, Dr. J. Edward Sunderland and Dr. John W. Hooper, are gratefully acknowledged. The author also would like to thank Messrs. C. R. Bannister, L. A. Cavalli, R. J. Collins, J. G. Doyle, J. W. Davis and D. W. Kiebel for their assistance in fabricating the experimental apparatus.

A special note of thanks is due the General Electric Company and General Motors, Inc. for their contributions of equipment.

The author also wishes to thank the Ford Foundation for the financial assistance which made this work possible.

TABLE OF CONTENTS

APPENDICES Page

LIST OF TABLES

LIST OF ILLUSTRATIONS

SUMMARY

An analytical and experimental investigation is presented in the area of magnetothermoelectricity, in particular the area of refrigeration or heat pumping.

The analytical portion of the investigation concerns the energy transfers resulting from the interaction of magnetic fields and electrical currents. The application of alternating currents, and consequently alternating magnetic fields, imposes many new phenomena not normally associated with direct current devices.

The analytical equations are developed from the theory of irreversible thermodynamics. Equations are determined for the temperature profiles, the Nernst-Ettinghausen and Fourier heat transfers, and coefficient of performances for heat pumps. Induced electric and magnetic polarization phenomena are considered in the analytical treatment and are shown to be negligible for the metal bismuth at low alternating frequencies (60 cycles per second). Introducing the induced currents in the expression for the total electric current reduces the alternating current equations to the direct current equations.

The analytical curves show that the temperature profile within the heat pump is greatly affected by an applied magnetic field. This temperature profile is used to calculate the quantity of Nernst-Ettinghausen heat, which is a function of the absolute temperature. Whereas, the gradient of the temperature profile is used to calculate the Fourier mode or conduction heat transfer.

An experimental apparatus was constructed to evaluate temperature profiles and heat transfers. The apparatus consisted of two separate electrical circuits, one for controlling the working electric current density through the test specimen and the second for control of the magnetic field strength. The test specimen represented the analytical model in every respect except for infinite length. Provision was made to eliminate thermal end effects by controlling the end temperatures. This was accomplished by water cooling the electric lead to bismuth interface of the test specimen.

Thermocouples were cast into the test specimen at time of construction and were used to measure the temperatures within the test sample and also the boundary conditions. The boundary conditions were maintained by a water cooling system. Thermocouples were also used to measure the exterior surface heat transfer by denoting the temperature difference in water circulating through the water jacket.

The electric working current was generated by large stepdown type transformers and the magnetizing field current was furnished by a variable transformer in series with a large industrial welding transformer. The electric working current could be varied from 0 to 1000 amperes. Also the induced magnetic field current had a range of 0-8000 amperes which permitted magnetic field variations from 0-1.2 kilogauss.

The test specimen was a long right circular cylinder constructed from reagent pure bismuth (99.98 per cent). The dimensions of the test specimen were: inside radius equal to 0.0127 meter, outside radius equal to 0.0254 meter and the length equal to 0.0762 meter.

Experimental data and analytical curves show very good agreement for the tests conducted. Experimental data points verify that the theory of irreversible thermodynamics can be expected to yield good results. The total experimental error is considered less than ±20 per cent. Of this, the systematic error is approximately ±15 per cent.

The results of this investigation show that alternating current Nernst-Ettinghausen heat pumps are possible, however they are not as practical as direct current heat pumps. The coefficient of performance for both alternating current and direct current heat pumps were compared and the results indicate that the effect of the eddy currents tends to reduce the coefficient of performance. The conventional heat production generated by eddy currents is negligible when compared to the effect of maintaining a one-dimensional heat flow. This effect becomes more prominent at high magnetic field strengths and low working currents.

A method of regulating the heat flux by phase angle control is developed. Initial experimental results indicate that the heat flux can be augmented, retarded or reversed by proper control of the relative phase angle between the electric current and magnetic field.

Recommendations are made on the initial designs for alternating current heat pumps. A new parameter called the zero eddy current radius must be considered in the design if the coefficient of performance is to approach the direct current heat pump.

The choice of direct current or alternating current should be based on the supply of the magnetic field and the supply for the work-

ing current. If an equal choice of power supply is allowed, the author suggests the application of direct current heat pumps because of the increase in coefficient of performance.

NOMENCLATURE

a	radius-inside, meter
A	area-cross sectional, m^2
A_e	Ettinghausen coefficient, m^3 °K/amp Weber
A_n	Nernst coefficient, m °K/amp
A_{ne}	Nernst-Ettinghausen coefficient, °K m^2/sec
b	radius-outside, meter
B	magnetic field, weber/m^2
C_o	constant, weber/amp m
C_1	specific heat, watt sec /kg °K
C_2	constant, Appendix B
C_3	constant, Appendix B
C_4	specific heat, watt sec/kg °K
C.O.P.	coefficient of performance
D	electric displacement, coulomb/m^2
e	thermoelectric power, volt/°K
e_v	energy, joule/kg
E	electric field, volts/m
EMF	electromotive force, volts
f	frequency, cycles per second
G	constant, Appendix B
H	magnetic displacement, amp/m
I	magnetizing current, amps
J	electric current, amp/m^2

$\bar{\bar{J}}$	energy fluxes, Appendix A
J_a	applied current, amps/m^2
J_e	eddy current, amps/m^2
k	thermal conductivity, watts/m °K
L	Leduc-Righi coefficient, m^2/volt sec
$\bar{\bar{L}}$	kinetic coefficients, Appendix A
m	specific magnetic polarization, volts/kg m
$\dot{m}$	mass flow rate, kg/hour
M	magnetic polarization, weber/m^2
p	specific electric polarization, volts/kg m
P	electric polarization, volts/m
P_e	average power-eddy, watts
$\bar{P}_e$	average power per unit volume per unit length, watts/m^4
q	heat flux, watts/m^2
q_{cond}	heat flux, Fourier, watts/m^2
q_{ne}	heat flux--Nernst-Ettinghausen, watts/m^2
Q	total heat flux, watts
r	space coordinate, meter
r_m	radius of zero eddy current line, meter
R	resistance, electrical, ohms
R_H	Hall coefficient, m^3/amp sec
s	entropy, joule/kg °K
t	time, second
T	temperature, °K
T_a	inside temperature at r = a, °K

T_b	outside temperature at r = b, °K
T_i	temperature of reservoir, °K
T_o	temperature of reservoir, °K
TC	thermocouple
u	internal energy, joule/kg
V	voltage, volts
V_i	initial volume, m^3
V_f	final volume, m^3
W	work, watts-sec
$\dot{W}$	power, watts
x	space coordinate, m
X	non-dimensional radius = r/b
$\bar{\bar{X}}$	affinities, Appendix A
X_m	non-dimensional eddy radius = r_m/b
y	space coordinate, m
Y	non-dimensional temperature = T/T_b
Y'	non-dimensional temperature = $(T - T_a)/(T_b - T_a)$
z	space coordinate, m
z_i	valence, dimensionless

Subscripts

Bi	bismuth
cu	copper
eq	equilibrium
m	mass
ne	Nernst-Ettinghausen

r	space coordinate
x	space coordinate
y	space coordinate
z	space coordinate

Greek Symbols

α	$2J_a C_o I A_{ne}/k$, dimensionless
α_e	$\omega\tau_e$, dimensionless
α_m	$\omega\tau_m$, dimensionless
α_o	constant, Chapter 5
β	$2GC_o I A_{ne}/k$, dimensionless
γ	$\rho_e(b^2/T_o k)$, dimensionless
ΔT	$T_b - T_a$, °K
ΔT_{wj}	$T_{\text{water inlet}} - T_{\text{water outlet}}$, °K
$\hat{\varepsilon}$	dielectric tensor, coulomb/volt m
ξ	energy flux, watts/m^2
η	kinetic coefficients, Appendix A
θ	space coordinate, radians
$\hat{\kappa}$	electric susceptibility, dimensionless
λ	kinetic coefficients, Appendix A
$\hat{\mu}$	magnetic permeability, weber amp/m
π_p	polarized terms, Appendix A
ρ_{cu}	electric resistivity, copper, ohms/m^3
ρ_e	electric charge density, coulomb/m^3
ρ_m	mass density, kg/m^3
ρ_r	electric resistivity, ohms m

σ_e	electric conductivity, mhos/m^3
σ_s	entropy, joule/kg ^oK
σ_m	entropy, magnetic, joule/kg ^oK
τ_v	volume, m^3
τ_e	relaxation time, electrical, seconds
τ_m	relaxation time, magnetic, seconds
$\hat{\chi}$	magnetic susceptibility, dimensionless
ω	angular frequency, rad/sec

CHAPTER I

INTRODUCTION AND HISTORICAL BACKGROUND

The conversion of energy from one form to a more useful form, the transfer of energy, and efficient utilization of energy are prime areas of interest to the engineer-scientist. The various mechanisms involved in energy conversion and transport may be categorized into many divisions, or fields. For example, the thermal to electrical field is concerned with the direct as well as the indirect conversion of heat to electrical power. A commercial steam power plant is an excellent example of the indirect method, i.e. thermal to mechanical and then to electrical. An example of the direct method from thermal to electrical is the simple thermocouple circuit.

The direct methods include the sub-field of thermoelectrics, among others. Thermoelectrics is a group of direct methods for converting thermal energy to electrical energy. If a magnetic field is added to thermoelectrics, the new conversion phenomena fall into the field of magnetothermoelectrics.

The analytical portion of this investigation concerns the energy transfers which result from the interaction of magnetic fields and electrical currents. The application of alternating currents, and consequently alternating magnetic fields, imposes many new phenomena not normally associated with direct current devices. In fact, all previous published investigations related to magnetothermoelectric conversion

devices have used direct current. Varga, et al., (1) suggested the use of alternating current but failed to mention the control possibility of the relative phase angle.

The purpose of this investigation is to analytically examine the utility and feasibility of alternating currents in magnetothermoelectric devices and then to experimentally verify the results by presenting a functional heat pump design. A bismuth alternating current heat pump which operates on the magnetothermoelectric principle is designed. Due to the Nernst-Ettinghausen effect, thermal energy is pumped from a low temperature source to a high temperature sink. The normal conduction heat, or Fourier heat, is imposed on the system by virtue of the temperatures at the boundaries. Since the Nernst-Ettinghausen effect resulting from the interaction of the magnetic field and the electric current is capable of pumping heat either in the direction of increasing temperature or in the direction of decreasing temperature, this paper is restricted to the conventional heat pump problem, namely, pumping energy in the direction of increasing temperature.

Magnetothermoelectric devices are now being considered for applications at low absolute temperatures since the device is simple and relatively cheap to make, has no moving parts, and requires almost no maintenance. The advantage of a magnetothermoelectric device over a thermoelectric device is that construction is simpler, since only one material is necessary, and the heat flow is perpendicular to the electrical current.

Related Literature Survey

Oersted (2) reported in 1829 that an electrical current carrying conductor will influence a nearby lodestone or steel magnet. In the same year Ampere (3) discovered that related forces between steel magnets arise from the presence of circulating currents within the material, which are now commonly called "Amperian Whirls." Ampere's original hypothesis has been shown to be essentially correct; the circulating currents in motion around the positive nuclei consist of the so-called "spinning" of the electron.

A year later Seebeck (2) observed that should a magnetized needle be placed near a circuit composed of at least two different electrical conducting materials, the needle is displaced when part of the circuit is maintained at a different temperature level than the rest. This well known effect is widely used today and is named after its observer, hence the Seebeck effect. In 1834, Peltier (4) discovered that if an electrical current is forced to flow in a closed circuit composed of at least two different conductors, a thermal gradient is established. This result is referred to as the Peltier effect, which is simply the inverse of the Seebeck effect. There are other effects associated with thermoelectrics (5), e.g., the Thomson heat, the Joule heat, etc.

Hall (6) first reported in 1879 that when an electrical current flows normal to a magnetic field in a conducting medium, a transverse electrical potential is established. The effect of this induced electrical field is called the "Hall effect." The discovery of this cross-phenomenon from the application of a magnetic field stimulated additional research in this field. In 1887 Ettinghausen (7) found that

for an isolated bar a thermal gradient was established perpendicular to the electric current when placed in a magnetic field. Nernst (8) demonstrated later that if thermal energy is made to flow through a conductor which is in a magnetic field, a transverse electric potential will be present. There are other effects which are not presented here, such as the Righi-Leduc effect where a thermal gradient is created normal to the heat flow in a magnetic field (8,9).

The Nernst effect and the Ettinghausen effect (7) are presented to demonstrate the Nernst-Ettinghausen effect. The Nernst effect is the variation or change in the thermal gradient in the direction of the electric current when a normal (perpendicular) magnetic field is applied. The Nernst coefficient is defined as the ratio of the temperature gradient in the axial direction to the axial electric current.

$$A_n = \frac{\partial T}{\partial z} / J_z \qquad (9) \qquad (1.1)$$

where T is absolute temperature, z is axial coordinate, and J_z is the electric current in axial direction.

The Ettinghausen effect is the appearance of a thermal gradient in an electric conductor which is mutually orthogonal to the directions of an applied magnetic field and an electric current. The Ettinghausen coefficient is defined as the ratio of the temperature gradient in the radial direction to the product of the magnetic field and electric current;

$$A_e = - \frac{\partial T}{\partial r} / B J_z , \qquad (1.2)$$

where B is the magnetic field and r is the radial coordinate.

The Nernst-Ettinghausen effect (9) which is used in the Nernst-Ettinghausen heat pump, is the appearance of an electric field mutually perpendicular to the thermal current and the applied magnetic field. The Nernst-Ettinghausen coefficient (Appendix A) is defined as the ratio of the electric field to the product of the radial temperature gradient and magnetic field.

$$A_{ne} = E_z / B \frac{\partial T}{\partial r} \qquad (1.3)$$

The first published information suggesting that the Ettinghausen effect could be used in heat pumping or refrigeration was made by O'Brien and Wallace (10) in 1957. They developed an optimum configuration for a maximum "efficiency." This shape is a tapered block with an exponential profile. They suggested using alternating current in a ring shaped device but no mention is made of alternating magnetic fields. Harman and Honig (11) published a two-part analysis of galvano-thermo-magnetic energy devices in 1962. The first part describes the equations for six different modes of energy conversion. Of particular significance is the transverse isothermal galvano-thermo-magnetic generator. The second part applies the theory to refrigerators and heat pumps, and also describes details for optimizing the coefficient of performance, geometry optimization for rectangular parallelopipeds and, in addition, some

limited experimental data. El-Saden (12) presented a thermodynamic analysis of the Ettinghausen cooler, however he and Harman and Honig (13) differ as to the energy flux at the cold interface. Delves (7) predicted that the photon drag effect (9) could perhaps be exploited to increase the cooling effect. Delves also published a theory for both intrinsic and extrinsic conductors and presented a practical design configuration. Paranjape and Levinger (14), and Horst (15) published analyses based on statistics and distribution functions.

In a recent paper Angrist (16) suggested using a Nernst effect in a power generator. One of the first to mention the use of alternating currents for both the magnetic field and the working electric current was Varga, et al., (1). This suggestion prompted the initial investigation of this subject. Recently an excellent study of Nernst-Ettinghausen refrigerators operating at room temperatures was presented by Harman, et al., (17). However, in all of the studies investigated, the author was unable to find any experimental or analytical work performed using both alternating currents and alternating magnetic fields in magnetothermoelectric heat pumps or refrigerators.

Present Investigation

The purpose of this study is to determine if a Nernst-Ettinghausen heat pump will operate on alternating current. In Chapter II the magnetothermoelectric phenomena is discussed and an analytical solution is obtained for the performance. The analysis considers the effects of induced polarization, the effects of induced currents, and the general overall performance for alternating heat pumps for right-

circular cylinder geometries.

An experimental investigation of a test specimen whose dimensions are identical to the analytical model except for length is presented in Chapter III. The radial temperature profile and the external surface heat transfer are measured with embedded thermocouples and a conventional heat balance is performed on the cooling jacket to determine the surface heat transfer.

In Chapter IV, the analytical and experimental results are discussed. Conclusions and recommendations of this study are presented in Chapter V.

CHAPTER II

ANALYTICAL INVESTIGATIONS

Mathematical Statement of the Problem

The purpose of this chapter is to analyze the alternating current magnetothermoelectric heat pump and to compare the output performance vis-a-vis the direct current devices. The radial temperature profile within the heat pump will be determined as well as the coefficient of performance.

A qualitative description of the magnetothermoelectric phenomena which occurs in Nernst-Ettinghausen heat pumps is presented first. A sketch of a simple Nernst-Ettinghausen heat pump is shown in Figure 1.

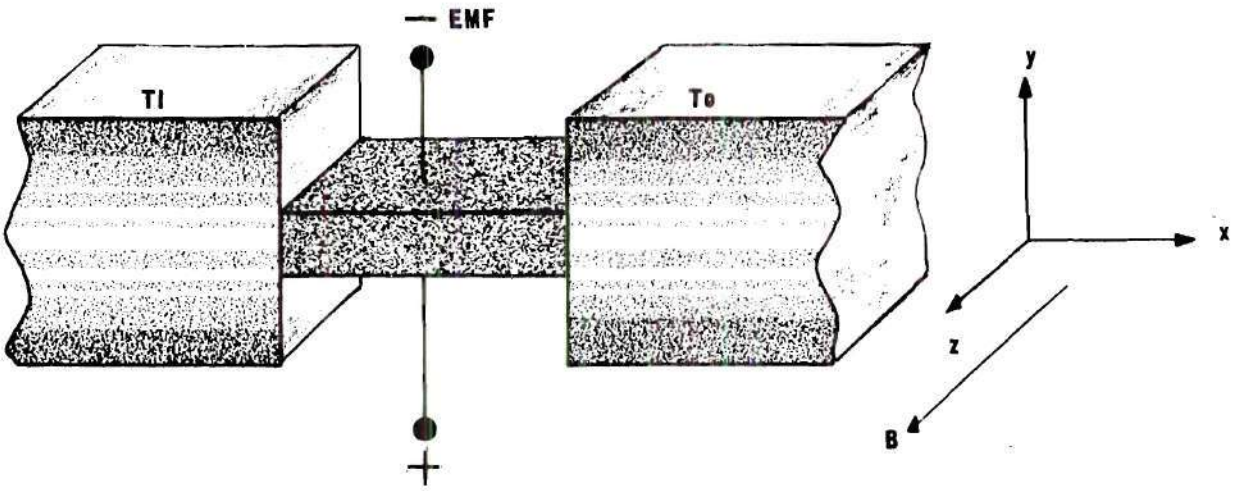

Figure 1. The Nernst-Ettinghausen Heat Pump

The heat pump is inserted between two reservoirs and connected electrically to a voltage source. The reservoirs are maintained at fixed temperatures $T_o > T_1$, and a magnetic field is applied in the positive z direction. The magnetothermoelectric material is placed between the two reservoirs and constructed of a material which has both holes and electrons for electrical conduction.

An electrical current flows along the positive y direction by virtue of the imposed EMF. Due to the reaction of charged particles moving in a magnetic field, both the holes and electrons achieve a velocity in the x-direction. This velocity is proportional to the product of the imposed electrical current and the magnetic field. The net effect is the creation of pairs of electrons and holes at one face and their destruction at the opposite face. Each pair carries energy and momentum across the material. The minimum energy required to displace an electron from its atom and thus permit it to move throughout the material is the energy gap(energy difference) between the bottom of the conduction band and the top of the valence band. This process of pair annihilation is called recombination. Impurity atoms produce localized electron and hole states that allow the process to occur. When an electron and hole combine, their energy and momentum are transferred to the lattice (18).

There are two mechanisms which contribute to the heat transfer: lattice vibrations and by motion of electrons and holes. When a magnetic field is applied, heat transfer due to the vibration mode remains approximately the same but that due to the charge carriers is greatly reduced (19). Electron-hole annihilation occurs at the warmer face while generation takes place at the colder face. Heat is liberated from this annihilation

and is absorbed by electron and hole generation. The device thus performs like a heat pump.

The heat pump shown in Figure 1 has an EMF and a magnetic field applied; however, no consideration had been given to the type of EMF or magnetic field. As was mentioned earlier, Varga, et al., (1) suggested that should the applied EMF (consequently the applied current) alternate at the same frequency as the magnetic field, their vector product, $\bar{J} \times \bar{B}$, would have only one sign and the result should be similar to the direct current problem.

Control of a direct current device requires adjustment of either the magnetic field or the working current. This must be accomplished by changing their magnitudes. However, it is not necessary to make magnitude adjustment on an alternating current device since regulation and control can be performed by varying the relative phase angle between the magnetic field and the working current. In fact, complete reversal in direction of the Nernst-Ettinghausen heat can be accomplished by a 180 degree phase shift.

The specific problem to be examined is a long hollow right circular cylindrical annulus. The alternating magnetic field, B, is produced in the angular direction and the alternating electric current, J, in the longitudinal direction. The analytical model is shown in Figure 2.

The development of the fundamental set of equations that apply to this problem is derived in Appendix A. The basis of this development is the theory of irreversible thermodynamics. The primary assumption used throughout is that the contribution to the entropy source term from

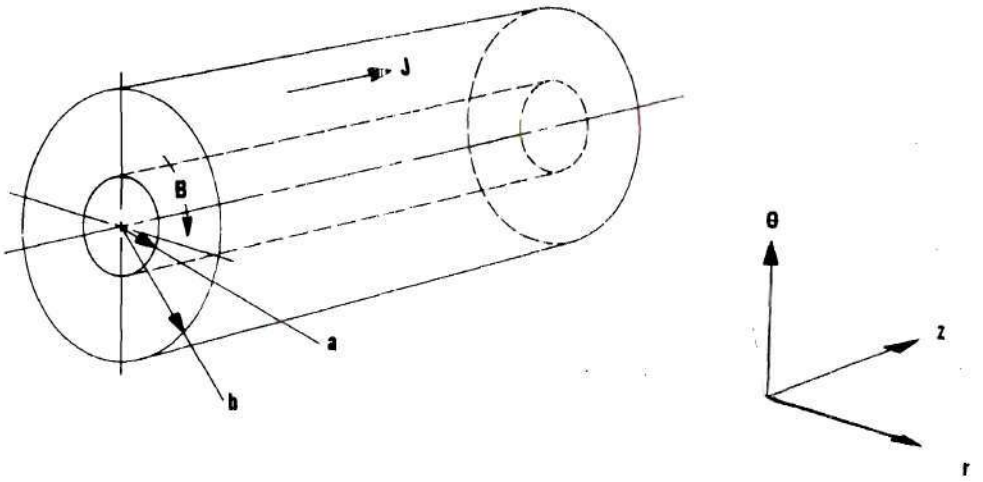

Figure 2. Analytical Model

the induced polarization phenomena resulting from applied alternating fields is considered small. These entropy source terms are a function of the difference in the induced fields and their associated equilibrium fields. It is seen that for relaxation times of order 10^{-9} seconds and for low frequencies, say less than 100 cps, the difference in the induced and equilibrium fields is of the order 10^{-7}. Hence, the induced polarization terms contributing to the entropy production may be neglected (Appendix A).

The equations are valid for thermal and electrical fluxes in a plane or surface normal to the applied magnetic field. A magnetic field is generated by passing a large alternating current, I, through the center of the cylinder parallel to the longitudinal axis. It is

represented by

$$B(r,t) = C_o(I \sin \omega t)/r \qquad (2.1)$$

where the constant C_o depends on the units selected for B, I and r.

An alternating electric current, J, is passed through the annulus collinear with the longitudinal axis. This electrical current is composed of two parts; the applied current and the induced eddy current,

$$J = J_a + J_e \ , \qquad (2.2)$$

where J_a is due to the applied electric field and J_e is a result of the alternating magnetic field.

The analytical model is infinite in the axial direction and finite in the radial direction. The inner radius is $r = a$ and the outer radius $r = b$. Since azimuthal symmetry is assumed, no variation is considered in the angular direction.

Using the above assumptions, the final equation resolves to a linear differential equation of second order and is solved in a conventional manner using numerical analysis by the Runge-Kutta technique (Appendix C) on a digital computer.

The properties of the material can be considered constant for the magnetic fields which will be applied. Harman and Honig (20) have shown that for magnetic field strengths below 10 kilogauss (1 weber/m^2) the Nernst-Ettinghausen coefficient is constant,

$$A_{ne} = E_z \,/\, B \frac{\partial T}{\partial r} \,. \qquad (A.54)$$

The increase in electrical resistivity of bismuth by a transverse magnetic field at 11.5 degrees centigrade is approximately 1 per cent for a 0.1 weber/meter^2 field and less than 3 per cent for a 0.2 weber/meter^2 field strength (21). The thermal conductivity also has a variation of less than 2 per cent for transverse fields less than 1.0 weber/meter^2 (21).

The general development considers the polarization phenomena and demonstrates that for the metal bismuth at low field frequencies (60 cps) this phenomenon is extremely small. The equations which represent the analytical model are (see Appendix A):

$$\begin{pmatrix} E_r \\ E_z \\ q_r \\ q_z \end{pmatrix} = \begin{pmatrix} \rho_r & +R_H B & -e & -A_{ne} B \\ -R_H B & \rho_r & A_{ne} B & -e \\ -eT & -A_{ne} BT & -k & -kBL \\ A_{ne} BT & -eT & +kBL & -k \end{pmatrix} \cdot \begin{pmatrix} J_r \\ J_z \\ \frac{\partial T}{\partial r} \\ \frac{\partial T}{\partial z} \end{pmatrix} \qquad (A.58)$$

where E is electric field, q is heat flux, R_H is the Hall coefficient, ρ is the electric **resistivity** , e is the thermoelectric power, k is the thermal conductivity, and L is the Leduc-Righi coefficient.

Because of infinite extent, the temperature gradient in the longitudinal direction is zero ($\partial T/\partial z = 0$). The total electric current is composed of the applied current and the induced current. The induced

current (eddy) is examined first.

Eddy Currents

If there is relative motion between an electrical conductor and a magnetic field, an induced electric current is produced. As will be shown, the effect of these currents is to reduce the performance. In this case the induced current is sometimes referred to as an eddy current.

The length of the mathematical model is infinite in the z-direction, therefore, the radial eddy currents are zero (Appendix B). However, the eddy currents in the axial direction are much different from zero. In order to understand this better, consider a metal conductor which is stationary within a moving magnetic field (Figure 3).

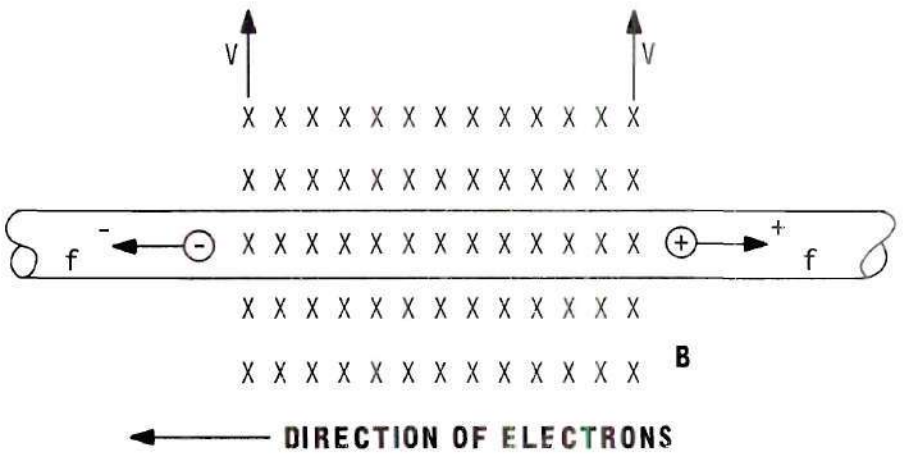

Figure 3. Electromagnetic Induction

The magnetic field has a direction into the page and a velocity v.

The forces on the free electrons (and holes) in the conductor are shown by the symbol f. If the ends of the wire are open, the movement of the electrons will cause the left end of the wire to become negatively charged, and the right end becomes positively charged. The reverse occurs when the field reduces (proceeds in the other direction) causing the electrons now to flow to the right and conversely for the holes. The flow of current is thus normal to the applied magnetic field (3).

It is now necessary to consider this longitudinal induced current. A profile of the eddy current is shown in Figure 4.

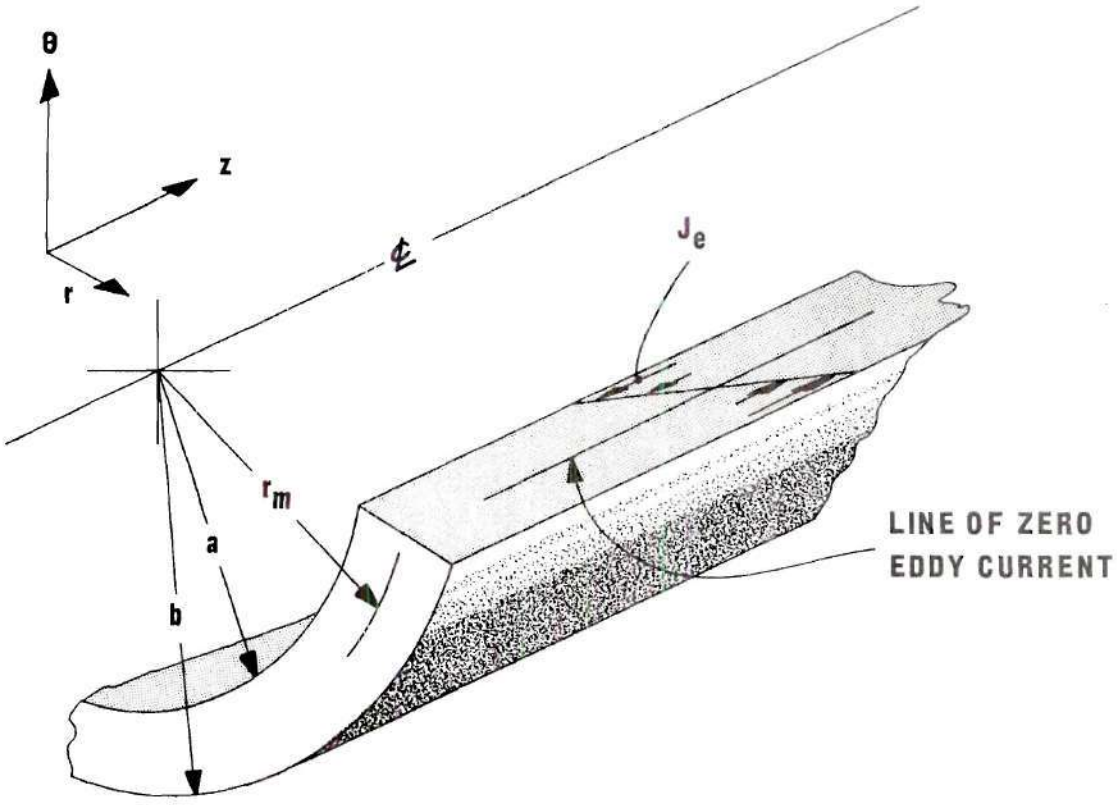

Figure 4. Eddy Currents

The eddy current profile is given for a particular instant of time. This current alternates or changes direction, depending on the direction of the magnetic field and is completely independent of any external circuit.

Since the total external flow of electrons is zero for the open circuit problem, the integral of the local induced current must be zero.

$$\int_r \int_\theta J_e \, r dr \, d\theta = 0 \qquad (B.17)$$

In order for the integral to be zero the sign (direction) of the induced current, J_e, must reverse between the radii. The radius where the induced current is zero is determined in Appendix B and depends on the geometry of the cylinder. This radius, r_m, is depicted in Figure 4.

Induced eddy currents are a direct result of alternating fields. Maxwell's equation is used to express the relationship.

$$\nabla \times \bar{E} = -\partial \bar{B}/\partial t \qquad (A.4)$$

Appendix B develops the expressions for the eddy currents and also locates the zero eddy current radius, r_m. The expression for the local longitudinal eddy current is

$$J_e = G \ln (r/r_m) \, . \qquad (B.9)$$

The expression for the local current density at any radius r is

$$J = J_a + G \ln (r/r_m) . \tag{2.3}$$

The J_r terms in equation A.58 are zero since the local radial eddy current is neglected and also there is no applied voltage in the radial direction. Applying the expressions for the magnetic field, the longitudinal current, and using the assumption of infinite axial length, the complex matrix set (A.58) reduces to the following set of equations:

$$\begin{aligned} E_r &= C_o R_H I J_z(\tfrac{1}{r}) - e \frac{\partial T}{\partial r} \\ E_z &= \rho_r J_z + A_{ne} C_o I(\frac{\partial T}{r \partial r}) \\ q_r &= -C_o I A_{ne} J_z \frac{T}{r} - k \frac{\partial T}{\partial r} \\ q_z &= -eTJ_z - C_o IkL \frac{1}{r} \frac{\partial T}{\partial r} \end{aligned} \tag{2.4}$$

Equations (2.4) represent the energy fluxes (watt/m^2) at any position (r,θ,z).

Equations (2.4) must now be applied to the relations developed as a result of the application of the first law of thermodynamics; namely, the conservation of energy principle. In the absence of any energy sources or sinks, the equation for the control volume (the cylinder) is written as:

$$\nabla \cdot \bar{\xi} = \frac{\partial}{\partial t}(\rho_m e_v)\Big|_{c.v.} \tag{2.5}$$

where $\bar{\xi}$ represents the total energy. The local mass density is ρ_m and e_v is the energy associated with this mass. The control volume element is

shown in Figure 5. The energy flux in the radial direction through the volume element is given by

$$\xi_r = (q_r + J_r V_r) \times A_r \tag{2.6}$$

where J_r is included for the present. Similarly, the energy flux in the longitudinal direction is

$$\xi_z = (q_z + J_z V_z) \times A_z \ . \tag{2.7}$$

Since axial symmetry is assumed, no variation is considered in the angular direction. The term V is the electrical potential difference (voltage).

Recalling that the electric current in the radial direction is zero, Equation (2.6) becomes

$$\xi_r = q_r A_r \ . \tag{2.8}$$

Applying the conservation of energy principle to the control volume element shown in Figure 5.

$$\xi_{r+\Delta r} - \xi_r + \xi_{z+\Delta z} - \xi_z = \rho_m C_1 \frac{\partial T}{\partial t} \Delta z r \Delta r \Delta\theta \tag{2.9}$$

The volume of the infinitesimal element is

$$\Delta vol = \Delta z \Delta r \, r \Delta\theta \ . \tag{2.10}$$

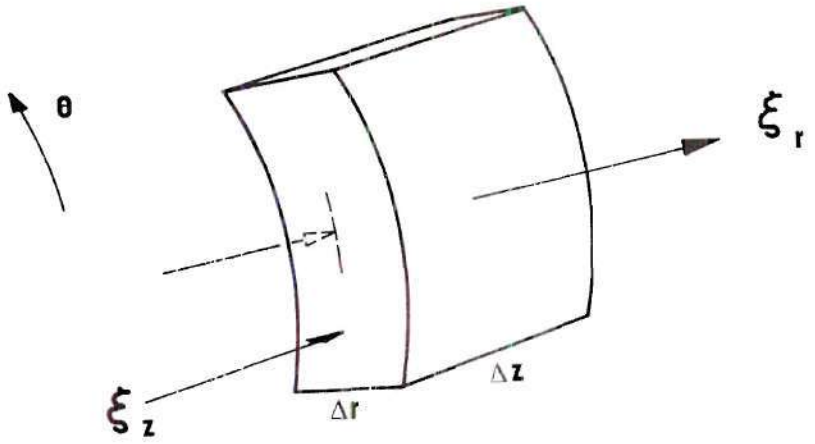

Figure 5. Control Volume Element

The term ξ_r represents the total energy per unit time entering the volume element in the r direction at the r location. Similarly $\xi_{r+\Delta r}$ represents the total energy leaving the volume element in the r direction at the r + Δr location. There is no energy entering or leaving the volume element from the angular direction since angular symmetry is assumed. The term ξ_z represents the total energy entering the volume element at the z location in the z direction, and similarly $\xi_{z+\Delta z}$ denotes the total energy leaving the volume element at the z + Δz location.

Substituting Equations (2.6) and (2.7) into (2.9) gives:

$$\frac{1}{r}\frac{\partial}{\partial r}(r\, q_r) + \frac{\partial}{\partial z}(q_z + J_z V_z) = \rho_m C_1 \frac{\partial T}{\partial t} \qquad (2.11)$$

Considering only the steady state case, and observing that $E_z = -\frac{\partial V}{\partial z}$, Equation (2.11) reduces to:

$$\frac{1}{r}\frac{d}{dr}(r\, q_r) - JE_z = 0 \qquad (2.12)$$

where J is given by Equation (2.3). Using Equations (2.4) for $-q_r$ and E_z in (2.13) gives:

$$\frac{1}{r}\frac{d}{dr}\left[r\left(-C_o I A_{ne} T(J_z + G\,\mathrm{Ln}(r/r_m)(\tfrac{1}{r}) + k\frac{dT}{dr}\right)\right] \qquad (2.13)$$

$$-(J_a + G\,\mathrm{Ln}(r/r_m))\left[\rho_r(J_a + G\,\mathrm{Ln}(r/r_m)) +\right.$$

$$\left. A_{ne} C_o I \frac{dT}{dr}(\tfrac{1}{r})\right] = 0$$

Introducing the non-dimensional variables

$Y = T/T_b$, where T_b is outside temperature

$X = r/b$, where b is outside radius,

the differential Equation (2.13) becomes

$$\frac{d^2Y}{dX^2} + \frac{1}{X}\frac{dY}{dX}[\alpha + \beta\,\mathrm{Ln}(X/X_m) + 1] + \frac{Y}{X^2}(0.5\beta) \qquad (2.14)$$

$$+ \gamma\,(J + G\,\mathrm{Ln}(X/X_m))^2 = 0,$$

where

$$\alpha = 2J_a C_o I A_{ne}/k$$

$$\beta = 2GC_o I A_{ne}/k \qquad (2.15)$$

$$\gamma = \rho_r (b^2/T_o\, k) \quad .$$

An examination of the above non-dimensional parameters reveals that α is a prime parameter since it involves J_a; β is the parameter which is a result of the eddy currents; and the parameter γ is the result of conventional joulean heating.

Using published values (Appendix G) for the properties in Equations (2.15), α, β, and γ may be calculated for the particular problem considered. Equation (2.14) is solved for the temperature distribution by the Runge-Kutta method of third-order accuracy (23). To use this technique, the initial derivative should be known; however, since only the temperatures at the boundaries, T_a and T_b were known, a procedure was developed in the computer program to first take a derivative of a predetermined value and then integrate the equation. The calculated boundary temperature was then compared with the given boundary condition. If the absolute value of their difference was less than 0.0001, the computer program calculated all the required data. However, if the boundary condition was not satisfied, a routine was used to adjust the initial derivative and then begin the entire integration procedure again. The initial derivative was adjusted until the boundary conditions were satisfied. All the temperature profiles pre-

sented in Figures 6-9 were determined in this manner. The computer program is given in Appendix C.

Once the temperature distribution has been determined, the radial heat flux at any location can be found from Equations (2.4). The heat flux in the radial direction is composed of two fluxes; the Nernst-Ettinghausen heat (24),

$$q_{ne} = -C_o I A_{ne} \, JT/r \tag{2.16}$$

and the conventional Fourier heat (24),

$$q_{cond} = -k \, dT/dr \; . \tag{2.17}$$

It should be noted that J and I are involved in Equation (2.16) and not in Equation (2.17). This fact is particularly useful for directing the flow of Nernst-Ettinghausen heat. By proper choice of relative phase angles of J and I, e.g. in phase or 180 degrees out of phase, the Nernst-Ettinghausen heat can be directed to flow independently of the imposed boundary conditions.

If the product of J times I is negative, then the heat flow is away from the center line (in the positive radial direction) against the imposed temperature rise. The specific purpose of a heat pump is to pump heat in direction of increasing temperature, therefore only this case (J x I is negative) is examined here.

The analytical results are shown in Figures 6-9 for given boundary conditions. The conditions are

$$T_{r=a} = 293.7\ ^{o}K\ ,$$

$$T_{r=b} = 296.2\ ^{o}K\ . \qquad (2.18)$$

The choice of the boundary conditions was predicated on the thermocouple emf derived from many experimental tests. The cooler temperature corresponded to 815 microvolts and the higher value to 915 microvolts. Figure 6 and 7 give the temperature as a function of the radius for an applied working current, J, with the magnetizing current, I, as a parameter. Figures 8 and 9 give the results using the applied current J as the parameter. The curves present results only for the case of heat being pumped in direction of increasing temperature. The temperature is plotted in terms of a non-dimensional temperature which varies from 0 at r = a to unity at r = b.

$$Y' = (Yx\ T_b - T_a) \ / \ (T_b - T_a) \qquad (2.19)$$

Once the temperature distribution has been determined, the radial heat flux at any position is found from the equation:

$$q_r = -C_o I A_{ne} J\ T(\frac{1}{r}) - k\ \frac{dT}{dr}\ , \qquad (2.4)$$

for the total heat transfer,

$$Q_r = q_r\ A_r\ . \qquad (2.20)$$

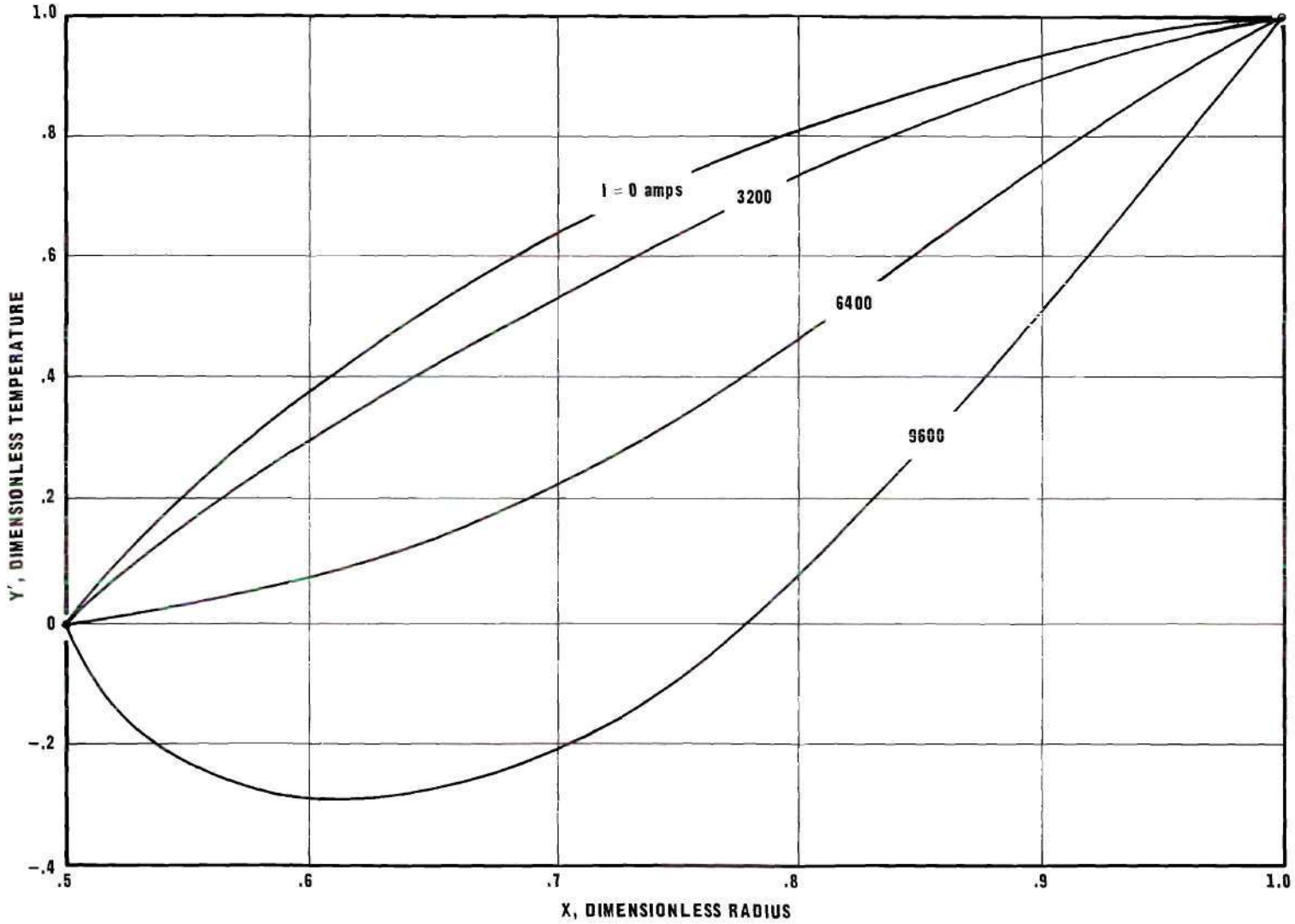

Figure 6. Temperature Profile for J = 3.29 x 10^5 amp/m^2 with Magnetizing Current as Parameter.

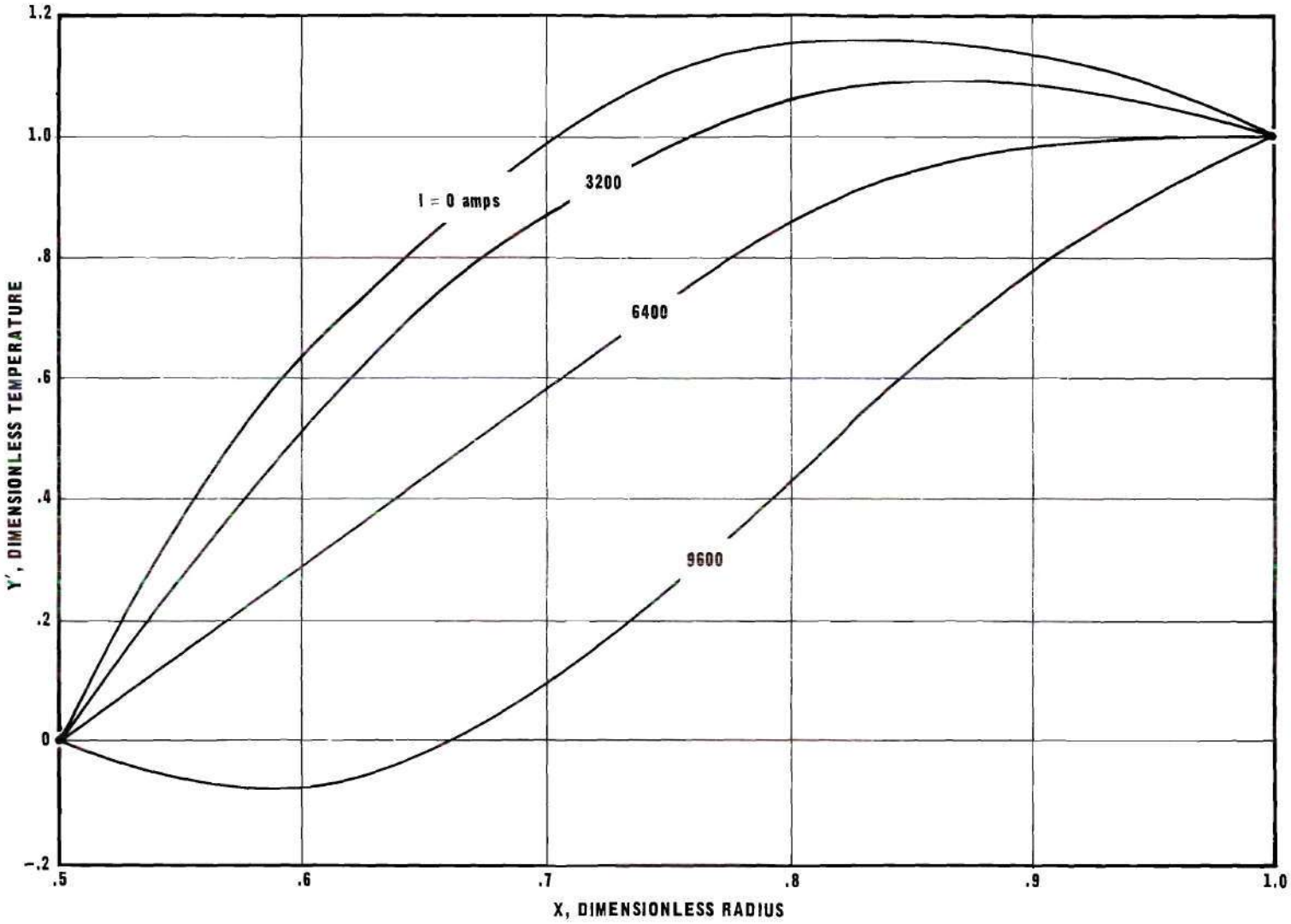

Figure 7. Temperature Profile for J = 6.58 x 10^5 amp/m^2 with Magnetizing Current as Parameter.

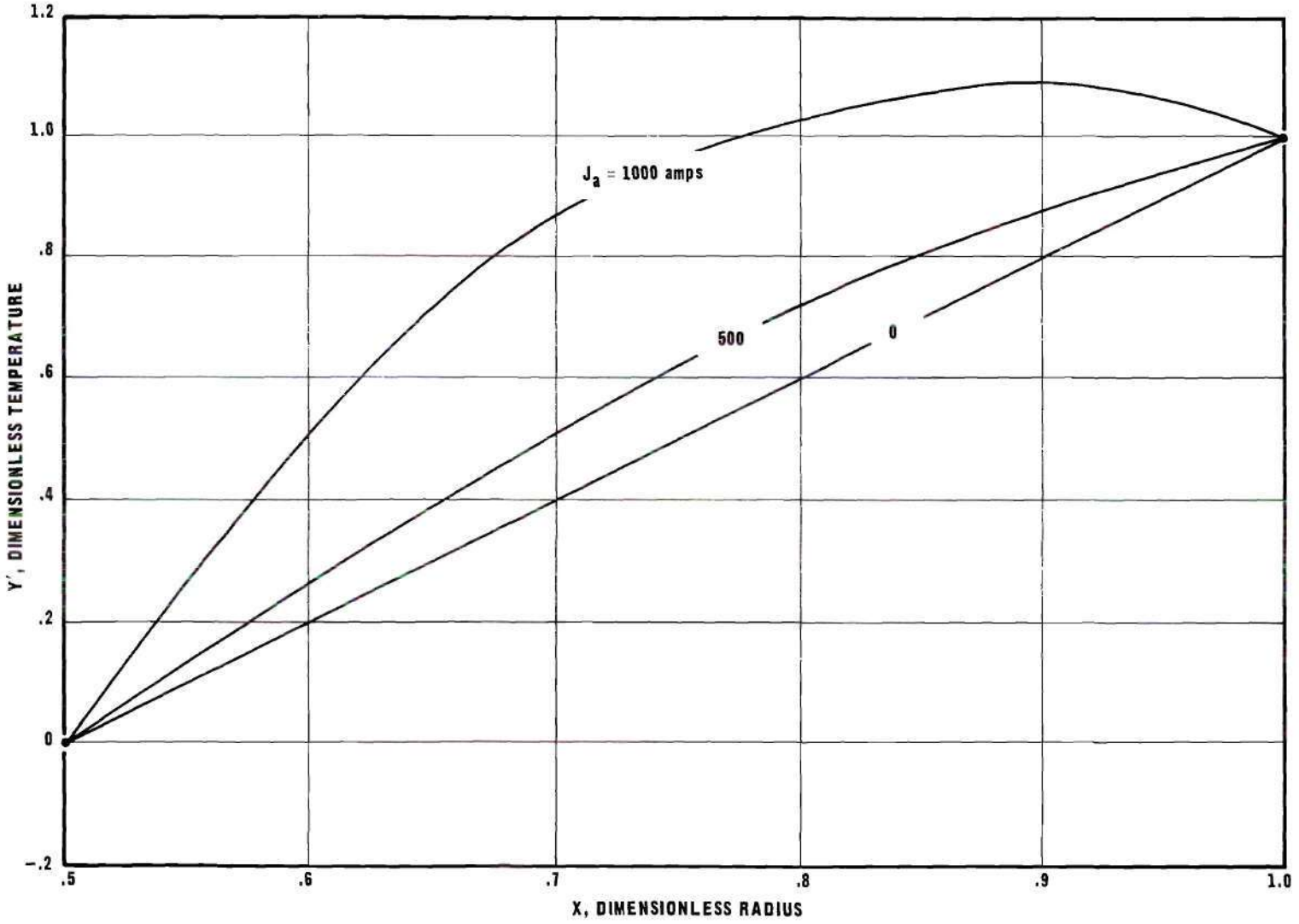

Figure 8. Temperature Profile for I = 3200 amps with Applied Current as Parameter.

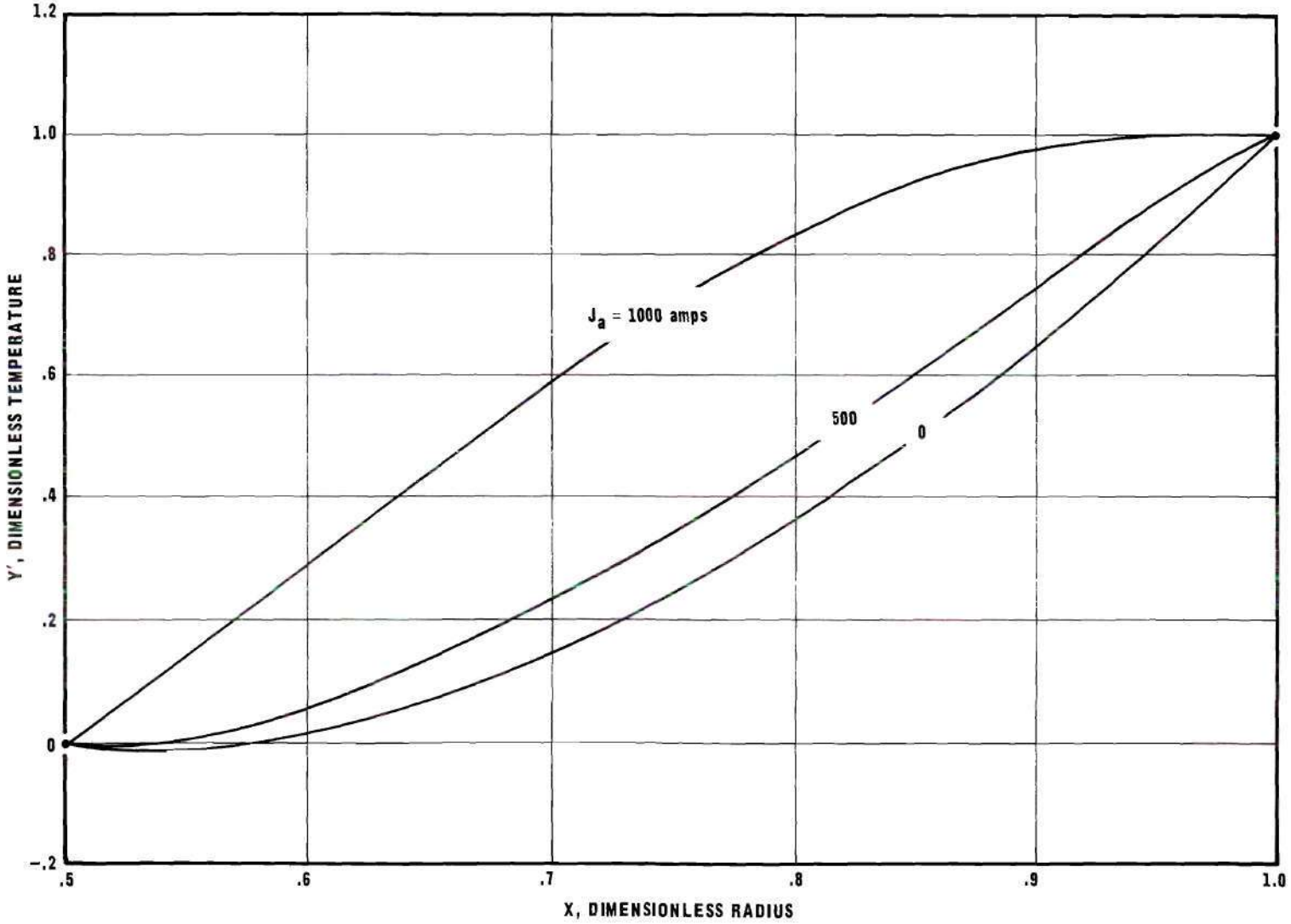

Figure 9. Temperature Profile for I = 6400 amps with Applied Current as Parameter.

Figure 10 gives the total heat transfer at the exterior radius, r = b for varying magnetic fields and with the applied current, J_a, as a parameter.

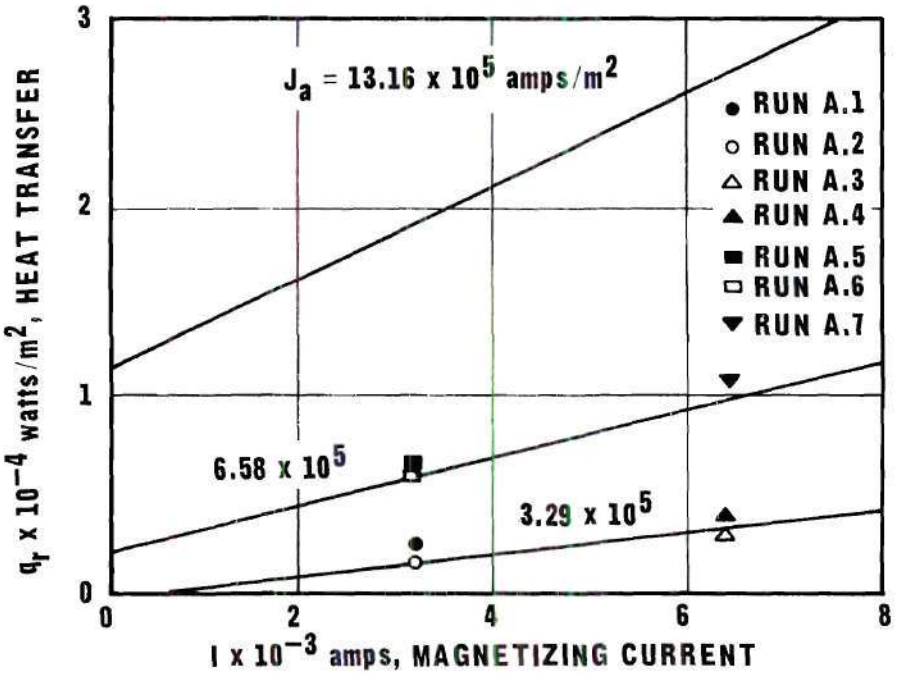

Figure 10. Heat Transfer at the Exterior Surface, r = b, for T_a = 293.7 °K, T_b = 296.2 °K.

Coefficient of Performance

The important criterion for examining any refrigeration device or heat pump is the overall coefficient of performance. The coefficient of performance of the heat pump is defined as the ratio of the heat pumped out of the system at the high temperature surface to the work required to achieve this pumping.

For a refrigerator, the C.O.P. is the ratio of the heat received at the low temperature surface to the work required to transfer this heat to the high temperature surface. Both heat pump and refrigerator coefficients have significance only if the thermal energy is being transferred into the system at the low temperature surface (24).

$$\underset{\text{Ref}}{\text{C.O.P.}} = Q_{r=a}/\text{Power input} \tag{2.21}$$

Applying the first law of thermodynamics to the control volume:

$$\sum_{\text{cycle}} \dot{W} = \sum_{\text{cycle}} Q = Q_{r=b} - Q_{r=a} \tag{2.22}$$

Introducing (2.22) into the expression for the coefficient of performance,

$$\underset{\text{Ref}}{\text{C.O.P.}} = 1/\left(\frac{Q_{r=b}}{Q_{r=a}} - 1\right) \quad . \tag{2.23}$$

Equation (2.23) is calculated for specific values of applied current density, $J_a = 3.29 \times 10^5$, 6.58×10^5 and 13.16×10^5 amp/m^2,

and the results are plotted in Figure 11. The curves show that the direct current device always has a higher coefficient of performance at any given magnetic field strength. That is, the effect of the induced eddy currents tends to reduce the overall performance of the heat pump. The curves for the low values of applied current diverge more rapidly for a given magnetizing current than the high values. This is reasonable since the induced eddy current created by the magnetic field is constant for any given magnetizing current and is a large percentage of the total amperage (Equation (2.2)) when the applied current is small.

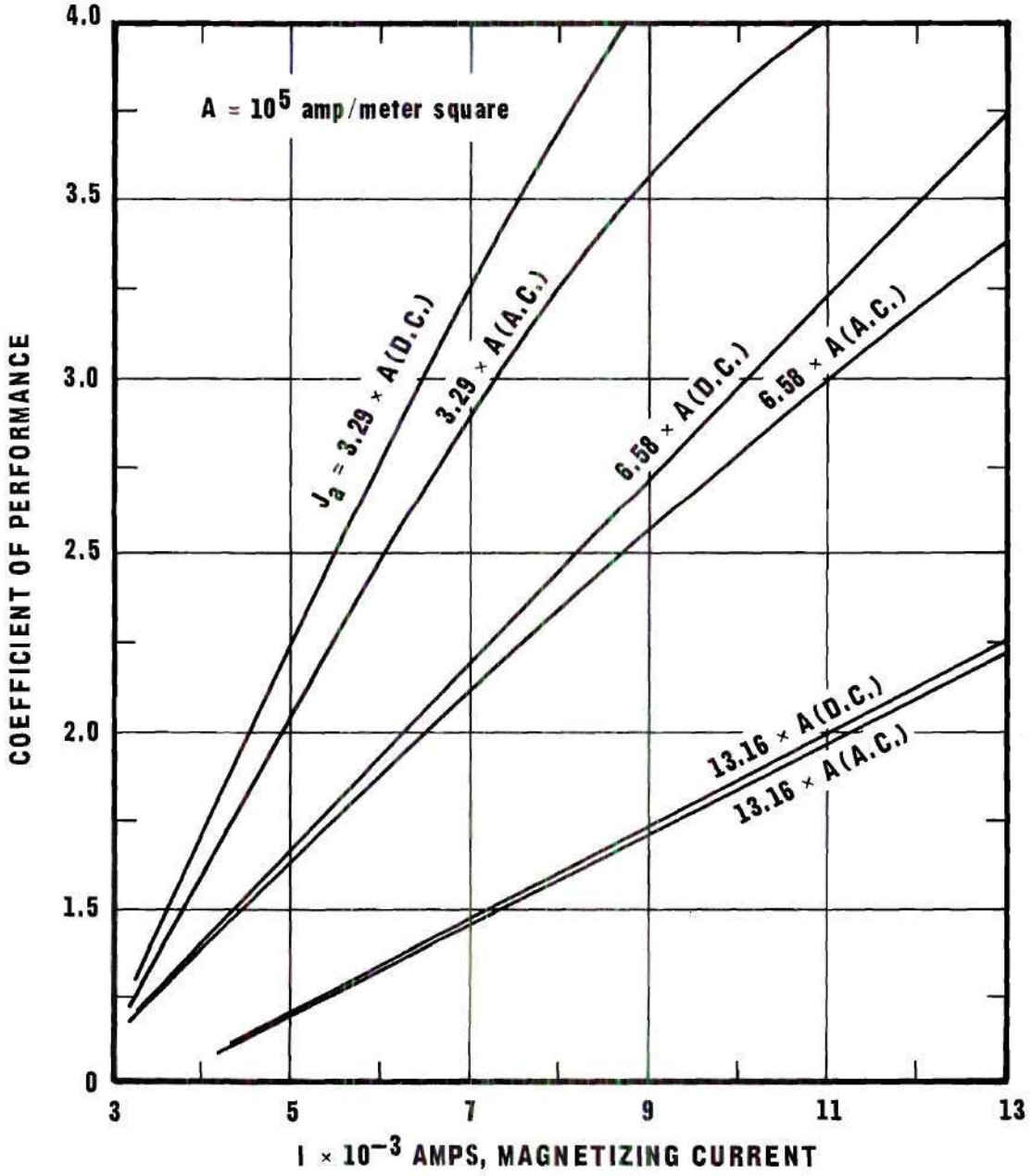

Figure 11. Coefficient of Performance vs. Magnetizing Current for Selected Values of Applied Current.

CHAPTER III

EXPERIMENTAL INVESTIGATIONS

The curves in Figures 6-9 show that the temperature profile within the heat pump is greatly affected by an applied magnetic field. This temperature profile must be known to calculate the Nernst-Ettinghausen heat, which is a function of the absolute temperature, and the Fourier heat, which is a function of the temperature gradient.

The purpose of this chapter is to describe the experimental apparatus and procedure used to determine this profile and to present actual test results. The validity of the analytical equations can be determined once the actual measured temperature profile is known.

The experimental arrangement for this investigation is shown pictorially in Figure 12. The apparatus consists of two separate electrical circuits; one for the production and control of the alternating magnetic field, the second for the control of the working electric current density, J, which passes through the test specimen.

Basically the requirement was to design a test system which is capable of producing large alternating magnetic fields without any large side effects, e.g. excessive heat production. The initial concept of large ferromagnetic coils for the field production was quickly discarded for two reasons; first, the high heat loss from hystersis effects and, second, the expense of an air gap electromagnet which would provide the required field. The idea of a circular field appeared

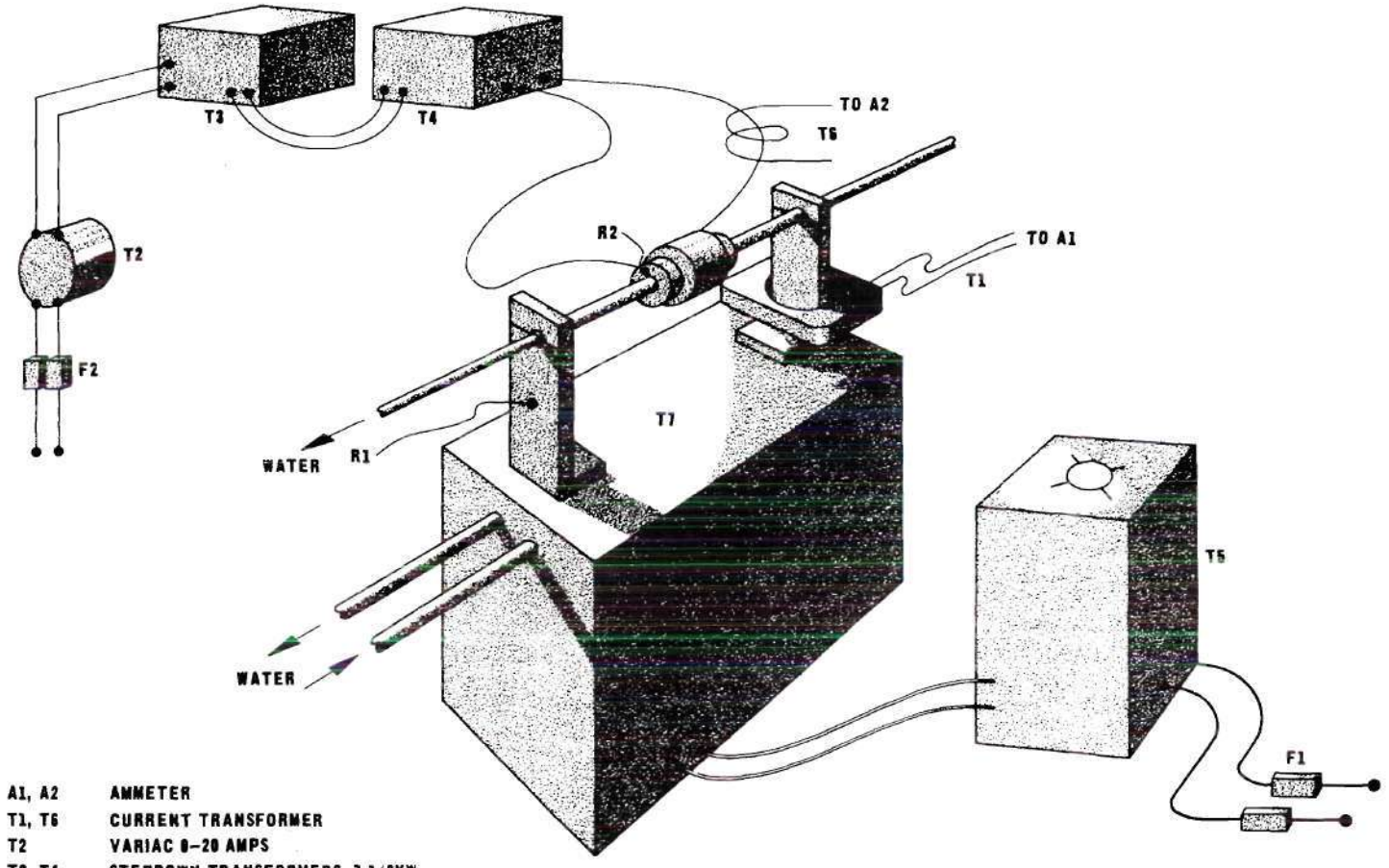

A1, A2	AMMETER
T1, T6	CURRENT TRANSFORMER
T2	VARIAC 0–20 AMPS
T3, T4	STEPDOWN TRANSFORMERS, 7-1/2KW
T5	VARIAC 0–240 AMPS
T7	WELDING TRANSFORMER, 75KW
F1, F2	FUSES
R1	COPPER BUS
R2	TEST SPECIMEN

Figure 12. Pictorial of Experimental Apparatus.

interesting and thus the final concept of a simple current filament to produce the applied magnetic field was used.

The magnetic field system was designed around a large welding-type industrial transformer. A large percentage of the test assembly was located on the top of this major piece of equipment (see Figure 12). A copper bus, 3' x 1', was designed to short circuit the transformer with a section machined to allow for the insertion of the test specimen. A current measuring transformer (8000 x 5) was installed around the bus to measure the current, I.

Although the copper bus short-circuited the transformer, there was still considerable heat production in the area of the test specimen because of the reduction in cross-sectional area. In order to maintain a thermal level near room temperature, a 1/8 inch diameter hole was drilled through the bus in order to water-cool the system. The entire bus assembly was brazed together to minimize any contact voltage drops. The input side of the welding transformer was connected to a variable transformer (auto-type), which was used to control the magnetizing current, I.

A long right circular cylinder was constructed from essentially pure bismuth. The constituents of the material are given in Appendix F. Bismuth was chosen primarily because of its magnetic, thermal, and electrical properties; a high Nernst-Ettinghausen coefficient, a low thermal conductivity, and a high electrical conductivity (25,26,27).

The dimensions of the test specimen were: inside radius equal to 0.0127 meter (1/2 inch), outside radius equal to 0.0254 meter and length equal to 0.0762 meter. Hence this configuration approached the mathe-

matical model if the assumption of infinite length was valid. The ratio of the length to thickness of six seemed at first to be sufficient, however, it was later found during the experimental investigations that a thermal gradient was produced from the high temperature copper leads connected to the test specimen. This problem was solved by water cooling the connections and inserting longitudinal thermocouples to monitor the axial temperature gradient. This arrangement proved very satisfactory. The axial thermal gradient could be held less than two degrees centigrade per meter. Therefore, the assumption of neglecting the end effects was considered acceptable. The only electrical problem resulting from finite length is the production of eddy currents in the radial direction. These eddy currents are small compared to the longitudinal eddy currents and, in fact, approached zero in the neighborhood of the thermocouples. The radial eddy currents, which are a result of the finite length, also produce a zero eddy current plane which is halfway between the ends of the bismuth specimen. The reason for this zero eddy current plane is identical to that for the zero eddy current radius.

The electrical circuit, which controlled the amount of working current, J, to the test specimen was connected to the same power supply as the welding transformer. Since both electrical circuits were supplied by the same voltage supply, the relative phase angle of the circuit was either 0 or 180 degrees depending on the electrical connections. The voltage output of the auto-transformer was stepped down (current stepped up) through two reduction -10:1 - transformers thereby producing a large secondary output current. The last transformer is

connected directly to the test specimen by large copper leads.

Figure 13 is a photograph of the actual test assembly in operation. Figure 14 is a schematic of the electrical circuits.

The thermal gradient within the bismuth test specimen must be accurately measured if the effect on the profile caused by the interaction of the induced magnetic field and the working current is to be determined. This interaction is seen to produce a lowering of the absolute temperature at any given point within the specimen (Figures 6-9).

The temperature profile was measured by using small copper-constantan thermocouples--0.008 inch diameter--arranged as shown in Figure 15. Figure 15 shows their location in the test specimen. Placing the thermocouples in this fashion greatly reduced any large errors due to thermal conduction. Analysis of this effect showed that the thermal conduction error was not larger than 0.05 °K. The thermocouples were constructed from the same stock of material to eliminate any metallurgical errors. Calibration of the thermocouple system was accomplished after assembly by placing the entire system into a water bath and comparing to a National Bureau of Standards immersion type thermometer.

A detailed error analysis is performed in Appendix D. This analysis considers the insertion of the thermocouples into the bismuth specimen. A computer study gives the error in the temperature profile caused by this foreign material as less than 4 per cent. The primary measurements of the electric currents and the location of the temperature sensing plane of the thermocouple are also considered and the

Figure 13. Photograph of Experimental Apparatus.

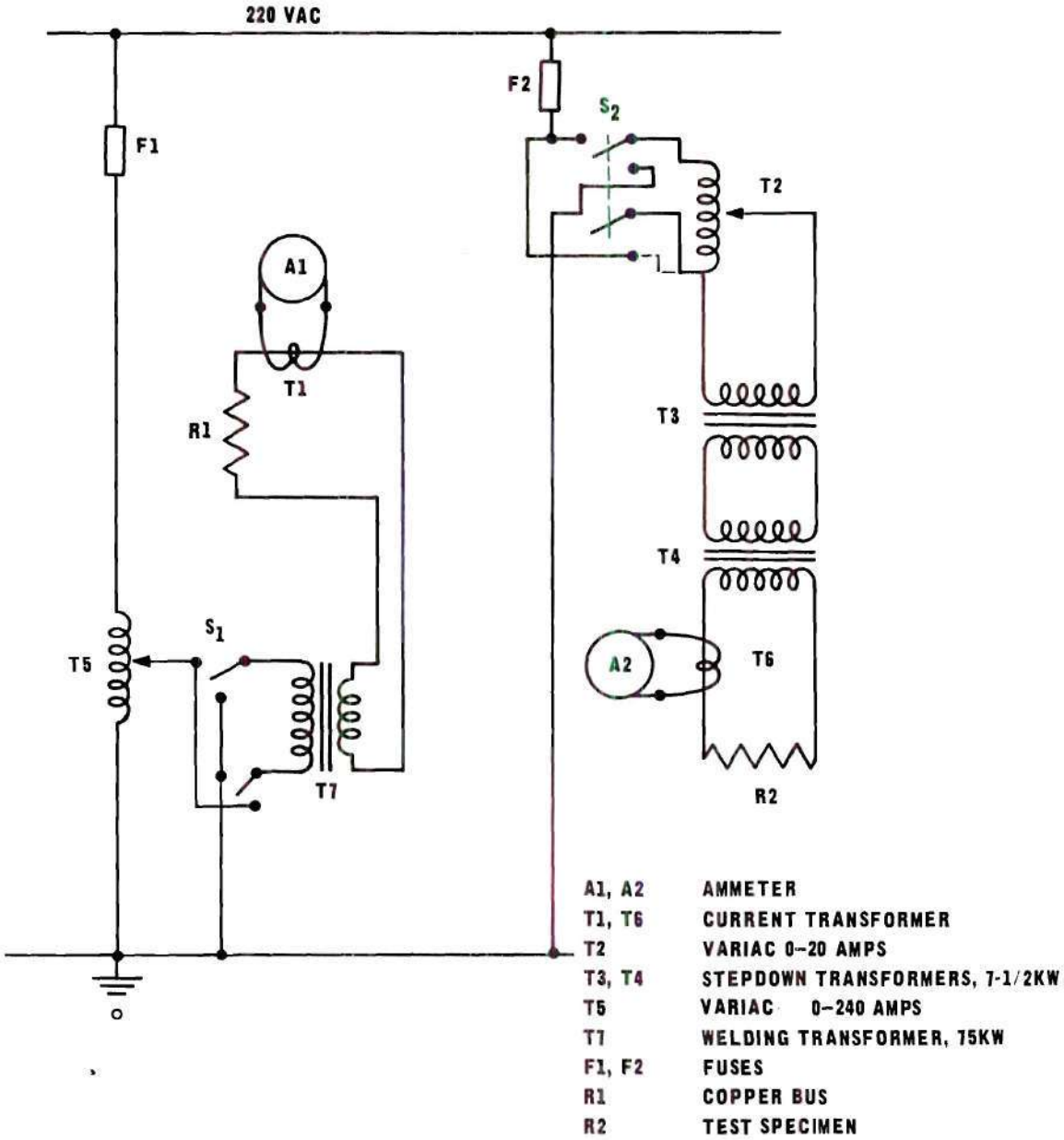

Figure 14. Electrical Circuit Diagram.

results indicate a possible variation of 11 per cent error. Considering all errors discussed, the most probable error of a temperature measurement is less than 20 per cent (see Appendix D).

After many attempts to locate the thermocouples in wells, slots, etc., the best solution was to form cast the test specimen around the thermocouple system. A three-part break-a-way mold was designed since bismuth has the property of expanding upon freezing, similar to water (28). The mold was made of a low carbon alloy steel and machined to the required dimensions. Each thermocouple was stretched across the center section (Figure 15) and secured before tightening the assembly with bolts. A paper grid was inserted between the two sections to assure the alignment of the thermocouples in the correct radial dimensions.

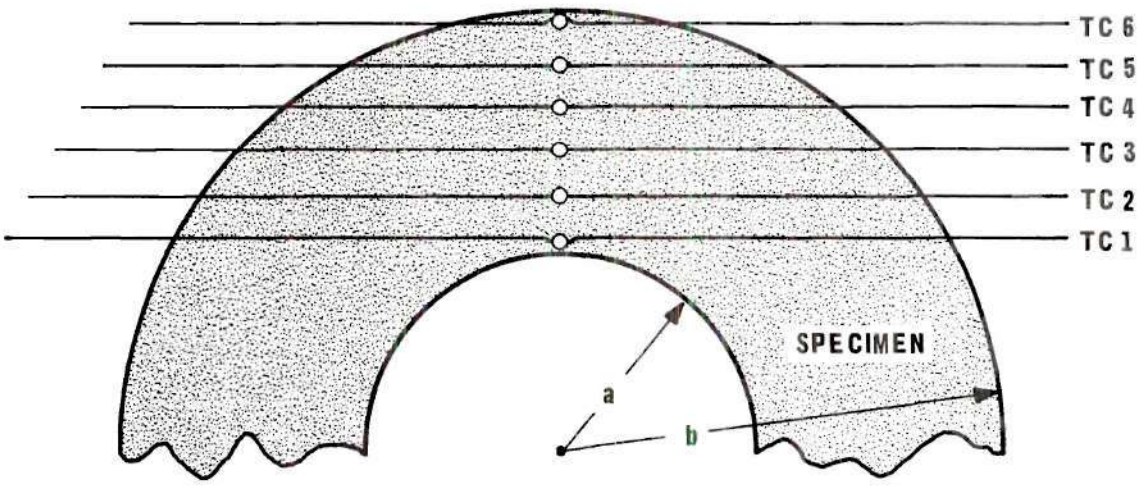

Figure 15. Location of Thermocouples

The mold and the bismuth were heated to around 500° C before the test specimen was poured. The heated mold helped in retarding any unusual crystal formations, e.g. gas holes, cracks, etc.

An attempt was made to determine the exact location of the thermocouple beads within the test section by radiography. A 50 millicurie supply of Cobalt 60 was used as the radiation source. It was desired to ascertain if any movement of the thermocouples had occurred during the setting-up process. This attempt failed in the initial purpose; however, it did verify that the test specimen was homogeneous and had no cracks or gas holes. The thermocouples could not be seen since the density path length for the bismuth-thermocouple path and the adjacent bismuth path were almost the same (29). Radiography is most effective when there is a large difference in the density of the object to be seen with respect to the density of the surroundings.

The test specimen was surrounded with a plastic water jacket in an effort to maintain a reference temperature at the surface. The water jacket, see Figure 16, was supplied by a pressure regulated water supply.

The exterior surface heat transfer was measured by inserting thermocouples in the input and outlet of the jacket. The mass flow rate of the water through the heat exchanger was determined by measuring the kilograms of water which emptied into a bucket in a given time interval (Table 1). Knowing the temperature difference, the specific heat and mass flow, the heat transfer at the exterior surface was calculated;

$$q_{r=b} = \dot{m}\, c_4\, \Delta\, T_{wj} \,. \qquad (3.1)$$

Table 1. Test Data for Exterior Surface Heat Transfer

Run Number	Applied Current (amps)	Magnetizing Current (amps)	Water Flow Rate (kg/min)	T_{in} (°C)	T_{out} (°C)
A.1	500	3200	1.1	21.70	21.95
A.2	500	3200	1.1	21.22	21.46
A.3	500	6400	1.1	25.02	25.57
A.4	500	6400	1.1	23.65	24.40
A.5	1000	3200	1.1	20.20	20.90
A.6	1000	3200	1.1	21.23	21.94
A.7	1000	6400	1.1	25.26	26.70

The specimen was placed around the copper bus and separated from electrical contact by thin mica strips. These strips are shown in Figure 16. After assembly the entire system was tested for electrical neutrality with respect to the magnetizing current circuit. The thermocouple leads were placed within spaghetti and completely insulated electrically. They were then bundled together and brought out through the plastic jacket at only one location to minimize any coolant leakage (Figure 17).

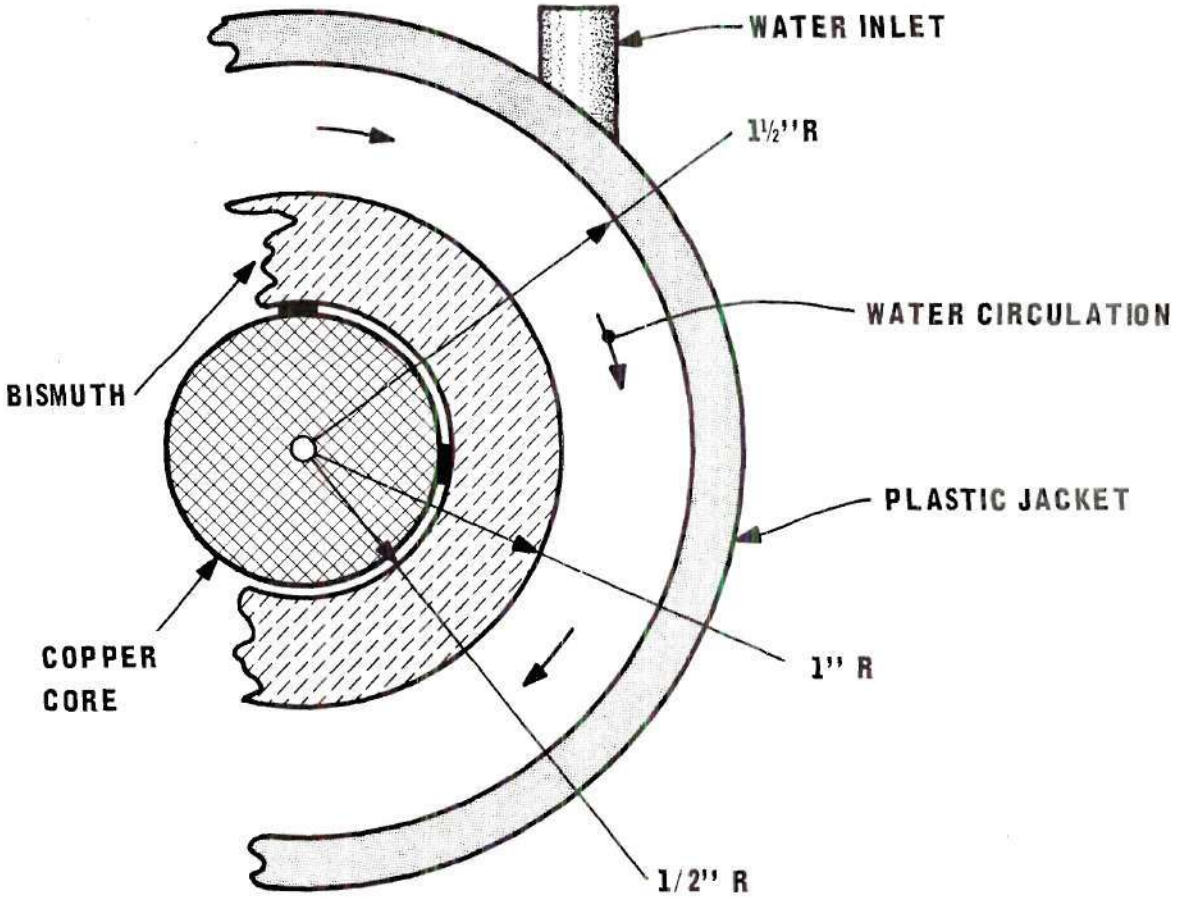

Figure 16. Cross-sectional View of Test Specimen and Water Jacket

The test results show very good agreement with the analytical results as indicated in Figure 10.

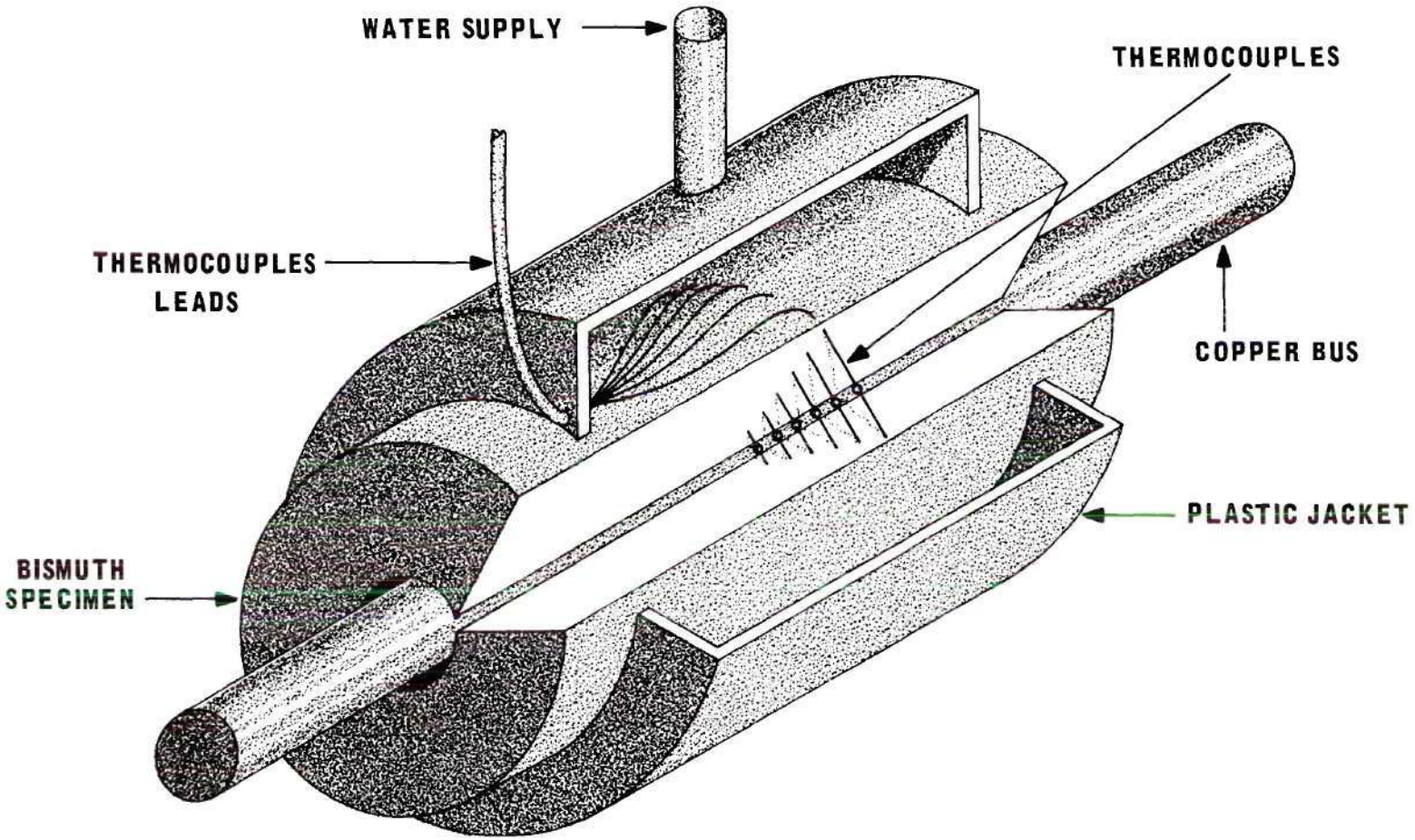

Figure 17. Cutaway of Test Specimen.

Experimental Procedure

The experimental procedure was to first allow the entire system to reach a thermal equilibrium state before any electrical power or magnetic field current was applied. Since the thermal level varied with the input power, the circulation of the cooling water both inside the cylinder, through the copper bus, and outside through the water jacket fixed the steady state temperatures of the system. The cooling water circulation was used to establish constant outside wall temperature of the test specimen at a value between 25 and 35° C.

The set of thermocouples was monitored during the initial cool-down and when no appreciable change was observed equilibrium was assumed. Technique was to change one of the two input variables, J or I, and observe the results. After either variable change, the system required two to three hours to attain steady state conditions. It was assumed that the system was in steady state, when a rate of change of temperature was less than 0.5 degrees per hour.

The values of the applied current used were: 0, 500, and 1000 amps which corresponded to a current density of 0, 3.29×10^5, 6.58×10^5 amp/m^2, respectively.

Table 2 gives the values of the observed temperatures for selected runs. The data are plotted also with the analytical curves in Figures 18 and 19. The experimental results show excellent agreement with the analytical profiles, especially in light of experimental error. The error band limits are derived in Appendix D. The total error is composed of two types, random and systematic. The random error, resulting from observation of instruments and fluctuating

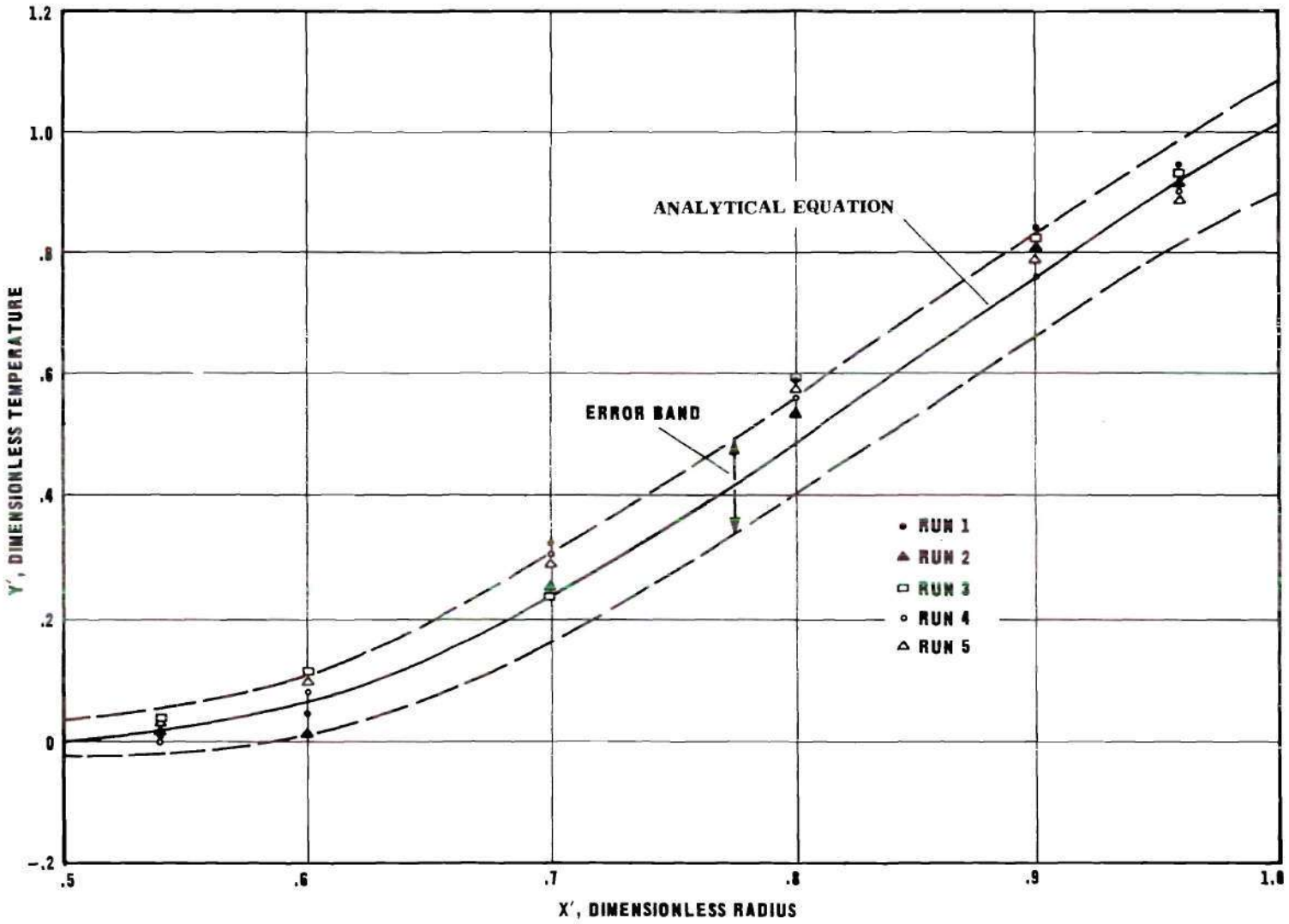

Figure 18. Temperature Profile for Magnetizing Current of 6400 amperes and J = 3.29 x 10^5 amps/m^2.

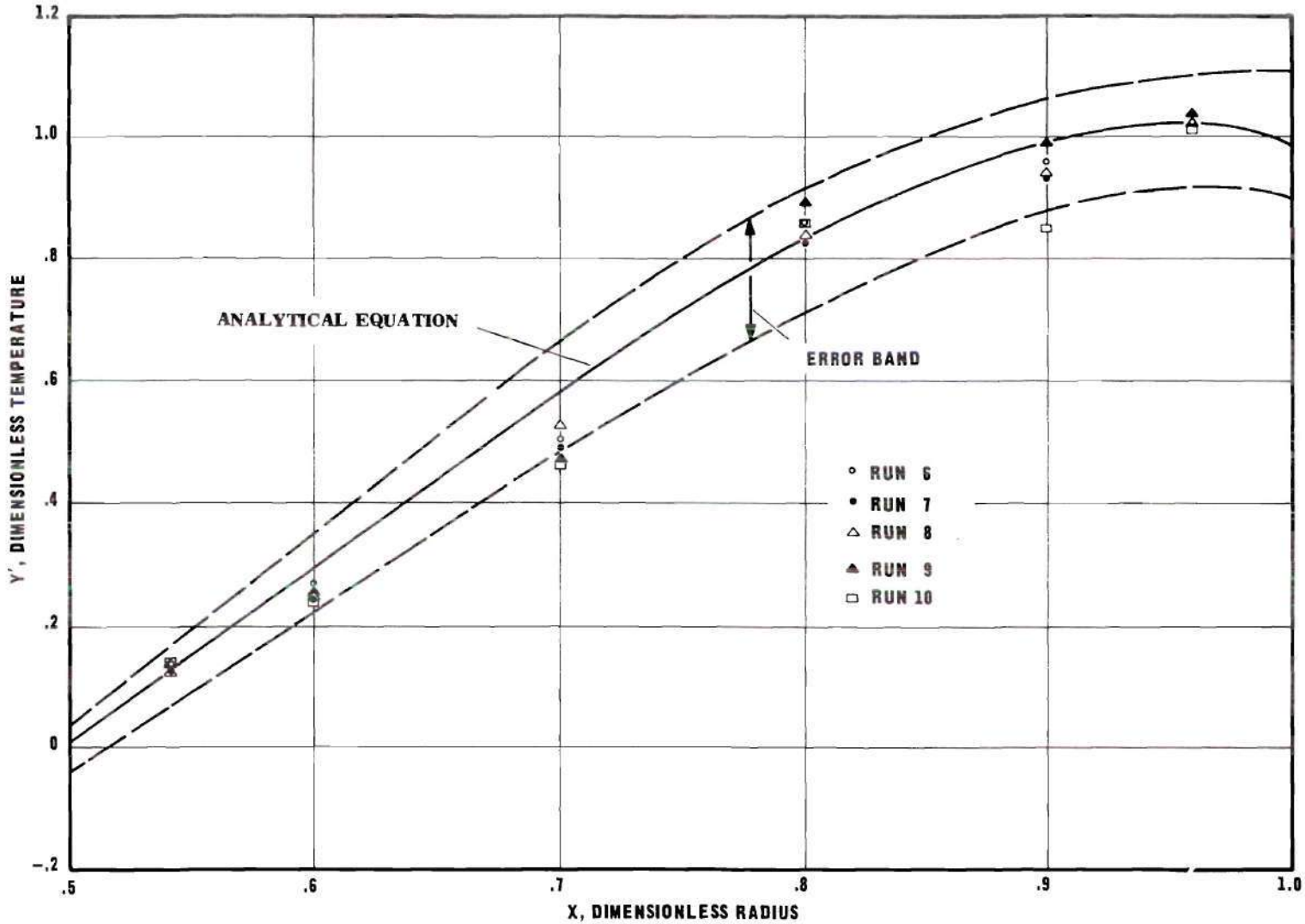

Figure 19. Temperature Profile for Magnetizing Current of 6400 amperes and J = 6.58 x 10^5 amps/m^2.

Table 2. Measured Temperature Profile Data

Run Number	Magnetizing Current (amps)	Working Current (Amps/m^2)	Temperatures (°C) 1	2	3	4	5	6
1	6400	3.29×10^5	27.55	27.90	29.70	31.58	31.83	32.45
2	6400	3.29	23.50	23.32	24.75	26.35	27.15	27.40
3	6400	3.29	22.00	22.33	22.95	24.45	24.60	24.95
4	6400	3.29	26.95	27.20	29.00	30.95	31.18	32.00
5	6400	3.29	26.50	26.80	27.80	29.00	29.10	29.50
6	6400	6.58	27.39	28.35	30.00	32.40	32.88	33.28
7	6400	6.58	28.50	29.40	31.10	33.50	34.00	34.50
8	6400	6.58	31.10	32.00	34.66	38.00	38.40	39.15
9	6400	6.58	31.70	32.40	33.20	35.30	36.10	36.05
10	6400	6.58	30.60	30.80	32.85	35.15	35.19	36.40

conditions, is less than 5 per cent. The systematic error, which is approximately 15 per cent results from three main sources; first, the location of the thermocouples; second, the insertion of foreign material as probes; third, the instrument accuracy measuring the magnetizing current and the working current.

CHAPTER IV

DISCUSSION OF RESULTS

Analytical and experimental temperature profiles have been obtained for an alternating current magnetothermoelectric heat pump. The measured data are given in Tables 1 and 2 and Figures 18 and 19. The analytical results are presented in Figures 6-9. As a typical result, the analytical curves in Figure 6 are for an applied current of 3.29×10^5 amps/m^2. The curve for zero magnetizing current, I = 0, is the temperature profile for simple Joulean heating. The other curves, I = 3200, 6400, and 9600, are presented to demonstrate the effect of the magnetic field on the temperature profile.

As the magnetic field current I is increased, the temperature profile tends to decrease until at the high strengths internal temperatures are lower than the boundary temperatures. The reason for this will be presented later. Therefore, with an increase in magnetic field, the absolute temperature is decreased. Figure 7 presents the profiles for a larger working current. The same relationship between temperature and magnetic field current exists.

Figures 8 and 9 demonstrate the effect of a variation in the working current for a constant magnetic field current. Figure 8 is for a magnetizing current of 3200 amps (0.5 kilogauss at r = a). Figure 9 is for a magnetizing current of 6400 amps (1.0 kilogauss at r = a). The curves clearly show that as the applied current is increased the

internal temperatures also increase. This is expected. The curves presented in Figure 11 give the effects of alternating fields. For comparison the profiles for direct currents (consequently steady magnetic fields) are shown with the alternating current profiles. The reducing effect of the eddy current is especially noted at the low applied currents. As an example, the effect of the eddy current is seen to reduce the coefficient of performance approximately 13 per cent for the conditions $J_a = 3.29 \times 10^5$ amp/m^2 and a magnetizing current of 9000 amps.

It should be noted that the temperature profiles shown in Figures 6-9 do not indicate the amount of heat transfer as in the case of normal conduction-Fourier mode-heat transfers. Thermal energy may be pumped either in the direction of increasing temperature or in the direction of decreasing temperature completely independent of the temperatures at the boundaries, at least ideally. The expression for the total heat transfer in the radial direction is

$$q_r = q_{ne} + q_{cond} . \tag{4.1}$$

The first term, q_{ne}, is the Nernst-Ettinghausen heat and is given by Equation (2.16). The second term, q_{cond}, is the conduction heat and is represented by Equation (2.17).

The Nernst-Ettinghausen heat is a function of the product of the working electric current density, J, and the local magnetic field strength, B. This product's algebraic sign determines the direction of the non-Fourier component in Equation (4.1). This direction is com-

pletely independent of the local temperature gradient. Hence, it is theoretically possible to construct a "perfect" adiabatic wall. The condition necessary is

$$q_{ne} = -q_{cond} \cdot \tag{4.2}$$

Examination of the curves in Figures 6-9 indicates that the temperature within the test specimen is always less in the presence of an alternating magnetic field than without a field. This phenomena can be explained by referring to Figure 20.

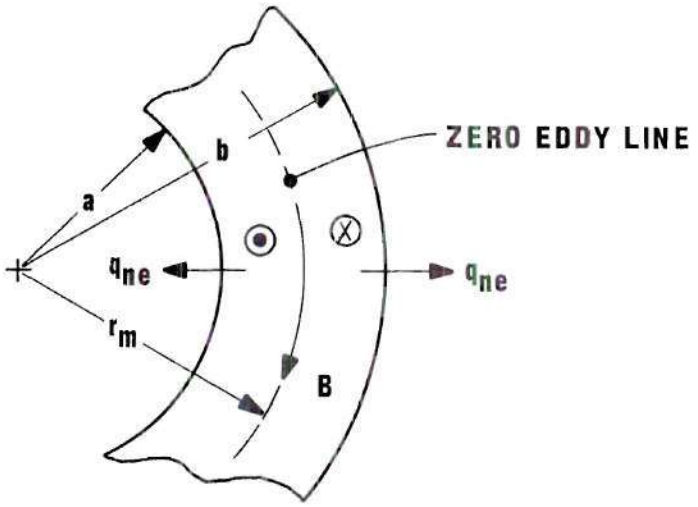

Figure 20. Effect of Induced Current.

The magnetic field B, is represented by an arrow and the local induced eddy currents by a dot or a cross depending on the direction. The dot indicates the current is out of the paper. A brief re-examination of Equation (2.16) shows that the product of the local current, in this case the eddy current, and the magnetic field determines the direction of the heat transfer. For bismuth, the Nernst-Ettinghausen heat is always directed away from the zero eddy current radius, r_m. Application of a magnetic field will lower the temperature within the specimen.

The actual experimental test results which are presented in Table 2 are plotted in Figures 18 and 19. The analytical analysis is verified within the accuracy of experimental measurements. It is seen from the figures that most observed experimental data fall within the most probable error limits.

The exterior heat transfer was determined both analytically (Figure 10) and experimentally (Table 1) and the results show excellent agreement. During the investigation the phase angle was reversed by 180 degrees to check if the cooling aspect would be present. This reversal was observed since the water temperature decreased as it passed through the jacket.

The experimental data and the analytical curves show very good agreement for the tests conducted. The actual data points tend to verify that the theory of irreversible thermodynamics can be expected to yield good results.

CHAPTER V

CONCLUSIONS AND RECOMMENDATIONS

The major conclusions that may be derived from this investigation are:

1. That alternating currents may be used in magnetothermoelectric devices provided the magnetic field also is alternating such that the produce of $\bar{J} \times \bar{B}$ is always of a singular sign, either positive or negative. This product is included in the expression (2.16), for the Nernst-Ettinghausen heat transfer, and to be of any significant value in heat pumping this product must be mono-directional.

2. That the heat transfer can be controlled and directed by varying the relative phase angle between the applied magnetic field and applied electric current. This technique affords a new and simple method for regulating magnetothermoelectric devices.

3. That direct current devices are capable of supplying more output heat for a given input work. This fact is best expressed by the coefficient of performance (Figure 11). It is seen that as the alternating magnetic field strength is increased the effect of eddy current production becomes quite significant.

4. That the theory of irreversible thermodynamics provides a basis for predicting the temperature profile and the direction of the total heat transfer.

5. That the C.O.P. for an alternating current device at zero

phase angle is small when compared to the Carnot C.O.P., however it is comparable to present day magnetothermoelectric and thermoelectric cooling systems. For example, a typical coefficient of performance for a parallelopiped as presented by Harman and Honig (11) may be found from their expression;

$$C.O.P. = \frac{293}{5}\left[\frac{1 - \sqrt{1-\alpha_o}\,\frac{(293)}{(288)}}{1 + \sqrt{1-\alpha_o}}\right] \qquad (5.1)$$

where α_o has been determined experimentally (39) for bismuth at 200 °K and in the presence of 5 weber/meter square as $\alpha_o = 0.40$. Applying this value to Equation (5.1) gives a C.O.P. of 4.60. These values however do not consider any expenditure of energy for the production of the magnetic fields. The Carnot coefficient for the hot temperature of 296.5 °K and a temperature difference of five degrees is approximately 66. The choice of five degrees is used since this is a reasonable temperature difference for the Nernst-Ettinghausen heat pump operating under load at the conditions used in the experimental tests.

The primary recommendations as a result of this investigation are:

1. That alternating current magnetothermoelectric devices be designed so that the effects of eddy currents will be small or negligible. This can be achieved by designing the system with thin laminations of magnetothermoelectric material. Each lamination must be separated by a low electric conductivity material which has a high

thermal conductivity. The thickness of the laminations will be determined by the cost of the construction. Since a zero eddy current line must be used to size the lamination, designs for right circular cylinders should include the expression:

$$\int_{r_1}^{r_2} \ln(r/r_m) r dr = 0 \ . \qquad \text{(B.18)}$$

If $r_2 - r_1$ can be made small, the effect of the eddy currents will be minor. It should be kept in mind however that the cost of manufacturing will increase rapidly as the lamination thickness becomes smaller.

2. The production of a large alternating current filament to produce the magnetic field in the experiments in this study was quite involved, both mechanically and electrically. The author recommends that consideration be given to producing this field using the coil method. In this method the production of the magnetic field strength is a function of the current and the number of turns of the coil.

3. That attempts to measure temperatures within solid metals use the concept of a single thermocouple wire with the other junction being the parent metal. Although this technique requires a more difficult calibration program, an expected advantage is that errors in temperature measurement will be reduced by at least 50 per cent. This would be significant for precision measurements.

APPENDICES

APPENDIX A

DERIVATION OF THE ENTROPY BALANCE EQUATIONS

The dynamic equations which represent the magnetothermoelectric phenomena in a polarized system are derived on the basis of irreversible thermodynamics. The theory of irreversible thermodynamics provides the general framework for the macroscopic description of the highly complex thermal-magnetic-electric phenomena. It provides the relationship between the forcing functions and the energy fluxes. This relationship, the entropy balance equation, relates the increase of entropy of a given control volume element from two primary causes; the net efflux of entropy from the control volume (the entropy leaving the control volume minus the entropy entering) and the internal production of entropy within the control volume as a result of the irreversible phenomena (22,30).

At present the theory is limited to linear departures from local equilibrium (31,32,33). However, this is sufficient since most transport relations are aptly described by linear relationships, Fick's law of diffusion, Fourier's law of heat conduction, etc. Therefore, the assumption of linear departures may be applied with good results expected.

In presenting this development, many definitions will be necessary. The terms and quantities are defined where needed and explained as the development progresses.

The use of alternating currents for controlling both the magnetizing field and the working electric current imposes many considerations not normally associated with direct current devices. First is the effect of polarization resulting from varying electric and magnetic fields. Therefore Maxwell's electric equations must be considered in the development of the dynamic equations. They are:

$$\text{Div } \bar{D} = \rho_e z_i \tag{A.1}$$

$$\text{Div } \bar{B} = 0 \tag{A.2}$$

$$\frac{\partial \bar{D}}{\partial t} - \text{Curl } \bar{H} = - \bar{J} \tag{A.3}$$

$$\frac{\partial \bar{B}}{\partial t} + \text{Curl } \bar{E} = 0 \tag{A.4}$$

The quantities $\bar{D}$ and $\bar{H}$ are the electric and magnetic displacement vectors. If the system is at rest, then these quantities are related to the magnetic and electric field strengths

$$\bar{D} = \hat{\varepsilon} \cdot \bar{E} \ , \tag{A.5}$$

$$\bar{H} = \hat{\mu}^{-1} \cdot \bar{B} \ , \tag{A.6}$$

where $\hat{\varepsilon}$ is the dielectric tensor and $\hat{\mu}$ the magnetic permeability tensor.

The electric polarization vector is defined as the difference of

the electric displacement and electric field vectors.

$$\bar{P} = \bar{D} - \bar{E} \tag{A.7}$$

The magnetic polarization vector is defined in a similar manner.

$$\bar{M} = \bar{B} - \bar{H} \tag{A.8}$$

Equation (A.7) may be further reduced by the definition

$$\hat{\kappa} = \bar{P}/\bar{E} \tag{A.9}$$

where $\hat{\kappa}$ is the electric susceptibility tensor. In an analogous fashion, the magnetic susceptibility tensor is defined as:

$$\hat{\chi} = \bar{M}/\bar{H} \ . \tag{A.10}$$

Substituting (A.9) and (A.10) into Equations (A.7) and (A.8), respectively gives:

$$\bar{D} = \bar{E}(\hat{\kappa} + 1) \tag{A.11}$$

$$\bar{B} = \bar{H}(\hat{\chi} + 1) \tag{A.12}$$

The vector equation, known as Poynting's theorem:

$$\nabla \cdot (\bar{E} \times \bar{H}) = +\bar{E} \cdot \frac{\partial \bar{D}}{\partial t} + \bar{H} \cdot \frac{\partial \bar{B}}{\partial t} + \bar{J} \cdot \bar{E} \qquad (A.14)$$

is derived by dotting the vector $\bar{H}$ into Equation (A.4) and by dotting the vector $\bar{E}$ into Equation (A.3), then adding. Equation (A.14) is used later in the analysis.

From the conservation of energy principle the energy change within a control volume per unit time is equal to the net efflux of energy across the boundaries of the control volume.

$$\frac{d}{dt} \int_{v_i}^{v_f} (\rho_m \, e_v) d \text{ Vol} = \begin{array}{l}\text{Rate of change of energy} \\ \text{within the control volume}\end{array} \qquad (A.15)$$

The local mass density is ρ_m and e_v is the energy associated with this mass.

Differentiation of (A.15) by Leibnitz's rule (34) gives

$$\int_{v_i}^{v_f} \frac{\partial}{\partial t} (\rho_m \, e_v) d \text{ Vol} + \rho_m \, e_v \Big|_{v_f} \frac{dv_f}{dt} - \rho_m \, e_v \Big|_{v_i} \frac{dv_i}{dt} . \qquad (A.16)$$

Applying the assumption that the volume does not vary with time, (A.16) reduces to:

$$\int^{\text{Vol}} \frac{\partial}{\partial t} (\rho_m \, e_v) d \text{ Vol} \qquad (A.17)$$

Excluding any nuclear effects, this change in energy of the control volume arises from the net efflux of energy across the system

boundaries, i.e.

$$-\int_{\text{Area}} \bar{\xi} \cdot d\bar{A} = \text{energy crossing boundary} \qquad \text{(A.18)}$$

Applying the divergence theorem and realizing that the equation must be valid for any arbitrary control volume, the result is that the integrand must therefore be zero.

$$\frac{\partial(\rho_m e_v)}{\partial t} = - \text{Div } (\bar{\xi}) \qquad \text{(A.19)}$$

Since the internal energy is composed of many energies, it is convenient to define the specific internal energy as:

$$u = e_v - \frac{1}{\rho_m} (1/2\ \bar{D} \cdot \bar{E} + 1/2\ \bar{B} \cdot \bar{H} - 1/2\ \bar{P} \cdot \bar{E} - 1/2\ \bar{M} \cdot \bar{B}) \qquad \text{(A.20)}$$

and also the heat flux $\bar{q}$ is defined as:

$$\bar{q} = \bar{\xi} - (\bar{E} \times \bar{H}) \quad . \qquad \text{(A.21)}$$

Substituting Equations (A.7) and (A.8) into (A.20) and inserting to (A.19) gives the balance equation for internal energy when the velocity is zero.

$$\rho_m \frac{du}{dt} = - \text{Div } \bar{q} + \bar{J} \cdot \bar{E} + \rho_m \bar{E} \cdot \frac{d\bar{p}}{dt} + \rho_m \bar{B} \cdot \frac{d\bar{m}}{dt} \qquad \text{(A.22)}$$

Recalling

$$\rho_m \frac{dq}{dt} = - \text{Div } \bar{q} \tag{A.23}$$

and applying the relation for the change of entropy for a reversible process (22,24):

$$dq = T\, ds \tag{A.24}$$

$$\rho_m T \frac{ds}{dt} = - \text{Div } (\bar{q}) \tag{A.25}$$

$$\rho_m \frac{du}{dt} = \rho_m T \frac{ds}{dt} + \rho_m \bar{B}_{eq} \cdot \frac{d\bar{m}}{dt} + \rho_m \bar{E}_{eq} \cdot \frac{d\bar{p}}{dt} \tag{A.26}$$

where the subscript, eq, indicates equilibrium conditions.

Recalling that Equation (A.22) is valid for the nonequilibrium condition, the expression for the entropy change is given when Equation (A.22) is subtracted from Equation (A.26).

$$\rho_m \frac{Tds}{dt} = - \text{Div } (\bar{q}) - \bar{J} \cdot (-\bar{E}) - \rho_m \frac{d\bar{p}}{dt} \cdot (\bar{E}_{eq} - \bar{E}) \tag{A.27}$$

$$- \rho_m \frac{d\bar{m}}{dt} \cdot (\bar{B}_{eq} - \bar{B})$$

$$\rho_m \frac{ds}{dt} = - \frac{\text{Div}}{T} (\bar{q}) + \frac{\bar{J} \cdot \bar{E}}{T} - \frac{\rho_m}{T} \frac{d\bar{p}}{dt} \cdot (\bar{E}_{eq} - \bar{E}) \tag{A.28}$$

$$- \frac{\rho_m}{T} \frac{d\bar{m}}{dt} \cdot (\bar{B}_{eq} - \bar{B})$$

The terms which are caused by the varying magnetic and electric fields are (the system is at rest and homogeneity is implied):

$$\pi_p = - \frac{\rho_m}{T} \frac{d\bar{p}}{dt} \cdot (\bar{E}_{eq} - \bar{E}) - \frac{\rho_m}{T} \frac{d\bar{m}}{dt} \cdot (\bar{B}_{eq} - \bar{B}) \qquad (A.29)$$

Equation (A.29) represents the entropy production from the irreversible phenomena associated with polarized systems. The magnitude of these terms will be shown to be inversely proportional to the relaxation times.

Considering the case of the magnetic relaxation, and noting that the electric relaxation is handled in a similar fashion, the expression for entropy production is:

$$\sigma_m = - \frac{1}{T} \frac{\partial \bar{M}}{\partial t} \cdot (\bar{B}_{eq} - \bar{B}) \qquad (A.30)$$

For an isotropic system the fundamental law for irreversible thermodynamics states that the linear phenomenological law corresponding to Equation (A.30) may be written (assuming small departures from equilibria),

$$\frac{\partial \bar{M}}{\partial t} = - \frac{L}{T} (\bar{B}_{eq} - B) = - \frac{L}{T\chi} (\bar{M} - \chi \bar{B}) \, . \qquad (A.31)$$

The inverse of the coefficient is generally referred to as the magnetic relaxation time, τ_m.

$$\frac{\partial \bar{M}}{\partial t} = - \frac{1}{\tau_m} (\bar{M} - \chi \bar{B}) \qquad (A.32)$$

In order to examine Equation (A.32), it is convenient to replace the magnetization vectors, $\bar{M}$, $\bar{B}$, by a Fourier transforms, namely

$$M(t) = \frac{1}{2\pi} \int_{-\infty}^{+\infty} \{\hat{M}(\omega)\, e^{-i\omega t}\} d\omega \qquad (A.33)$$

$$B(t) = \frac{1}{2\pi} \int_{-\infty}^{+\infty} \{\hat{B}(\omega)\, e^{-i\omega t}\} d\omega \qquad (A.34)$$

The insertion of (A.33) and (A.34) into (A.31) gives

$$- \frac{i\omega}{2\pi} \int_{-\infty}^{\infty} M(\omega)\, e^{-i\omega t} d\omega = - \frac{1}{2\pi} \int_{-\infty}^{\infty} (\hat{M}(\omega) - \chi \hat{B}) e^{-i\omega t} d\omega \qquad (A.35)$$

Removing the integral sign and clearing:

$$\tau_m i\, \omega \hat{M} - \hat{M} + \chi \hat{B} = 0 \qquad (A.36)$$

Since $\hat{M} = \hat{\chi}\hat{B}$, Equation (A.36) becomes

$$\hat{\chi} = \frac{\chi}{(1 - i\omega\, \tau_m)} = \frac{\chi}{(1 - i\alpha_m)} . \qquad (A.37)$$

A similar relationship is also developed for the electrical susceptibility:

$$\hat{\kappa} = \frac{\kappa}{(1 - i\omega \tau_e)} = \frac{\kappa}{(1 - i\alpha_e)} \qquad (A.38)$$

It is seen that if α_e is much smaller than unity, the polarized susceptibility reduces to the static case. For example, these conditions exist if the relaxation times are slow. The relaxation time for bismuth is of the order 10^{-11} (35) and if the applied frequency is small--60 cps--then α_e is order 10^{-9} (35).

Since this investigation considers only 60 cycles per second fields, the electric and magnetic tensors reduce to the isotropic scalars, i.e.

$$\hat{\chi} = \chi \ , \quad \hat{\kappa} = \kappa \qquad (A.39)$$

It is seen that for the low frequencies involved in this experiment the static fields are assumed to be equal to the non-equilibrium fields and therefore the entropy producing terms due to polarization phenomena are zero.

$$\frac{1}{T} \rho_m \frac{d\bar{p}}{dt} \cdot (\bar{E} - \bar{E}_{eq}) = \frac{1}{T} \rho_m \frac{d\bar{m}}{dt} \cdot (\bar{B} - \bar{B}_{eq}) = 0 \qquad (A.40)$$

Rewriting the entropy balance Equation (A.28) and expressing the term for thermal flux in a different form by using the relation,

$$\text{Div } (\bar{q}/T) = (\text{Div } \bar{q})T + \bar{q} \cdot \text{Grad } (1/T) \ , \qquad (A.41)$$

the following equation for the entropy source is obtained:

$$\sigma_s = \frac{ds}{dt} + \text{Div}\ (\bar{q}/T) = \bar{q} \cdot \text{Grad}\ (1/T) + \frac{\bar{J} \cdot \bar{E}}{T} \qquad (A.42)$$

This equation gives the appropriate fluxes and affinities to develop the necessary linear relationships from the theory of irreversible thermodynamics. This theory may be stated as:

> It is known empirically that for a large class of irreversible phenomena and under a wide range of experimental conditions, the irreversible flows are linear functions of the thermodynamics forces, as expressed by the phenomenological theories of irreversible processes. Thus, e.g. Fourier's law for heat conduction expresses that the components of the heat flow are linear functions of the components of the temperature gradient and Fick's law establishes a linear relation between the diffusion flow of matter and the concentration gradient. Also included in this kind of description are the laws for such cross-phenomena as thermal diffusion, in which the diffusion flow depends linearly on both the concentration and temperature gradients. If we restrict ourselves to this linear region we may write quite generally

$$\bar{\bar{J}}_i = \sum_k \bar{\bar{L}}_{ik}\, \bar{\bar{X}}_k \ , \qquad (1)$$

> where $\bar{\bar{J}}_i$ and $\bar{\bar{X}}_i$ are any of the Cartesian components of the independent fluxes and thermodynamic forces appearing in the expression for the entropy production, which is of the form

$$\sigma_s = \sum_i \bar{\bar{J}}_i\, \bar{\bar{X}}_i \ .$$

> The quantities $\bar{\bar{L}}_{ik}$ are called the phenomenological coefficients and (1) will be referred to as the phenomenological equations. (30)

Applying the above theory to the entropy equation (A.42) the following matrix equation is obtained:

$$\begin{pmatrix} J_r \\ J_z \\ q_r \\ q_z \end{pmatrix} = \begin{pmatrix} \eta_{11} & \eta_{12} & \eta_{13} & \eta_{14} \\ \eta_{21} & \eta_{22} & \eta_{23} & \eta_{24} \\ \eta_{31} & \eta_{32} & \eta_{33} & \eta_{34} \\ \eta_{41} & \eta_{42} & \eta_{43} & \eta_{44} \end{pmatrix} \cdot \begin{pmatrix} E_r/T \\ E_z/T \\ \frac{\partial}{\partial r}(1/T) \\ \frac{\partial}{\partial z}(1/T) \end{pmatrix} \tag{A.43}$$

The utility of Equation (A.43) is greatly increased if the experimentally controlled variable, J, is placed on the right side and the factors T and $-1/T^2$ are included in the new kinetic coefficients. Inverting Equation (A.43),

$$\begin{pmatrix} E_r \\ E_z \\ q_r \\ q_z \end{pmatrix} = \begin{pmatrix} \lambda_{11} & \lambda_{12} & \lambda_{13} & \lambda_{14} \\ \lambda_{12} & \lambda_{11} & \lambda_{14} & \lambda_{13} \\ T\lambda_{13} & T\lambda_{14} & \lambda_{33} & \lambda_{34} \\ T\lambda_{14} & T\lambda_{13} & \lambda_{34} & \lambda_{33} \end{pmatrix} \cdot \begin{pmatrix} J_r \\ J_z \\ \partial T/\partial r \\ \partial T/\partial z \end{pmatrix} \tag{A.44}$$

where the new coefficients are functions of η_{ij} and the temperature. The first coefficient λ_{11} is related as

$$\lambda_{11} = \frac{\eta_{11} T}{(\eta_{11}^2 + \eta_{12}^2)} \quad . \tag{A.45}$$

The kinetic coefficients are now replaced by the descriptive coefficients which are defined as:

The absolute thermoelectric power,

$$e = -E_r / \frac{\partial T}{\partial r} , \quad \text{when} \quad J_r = J_z = \frac{\partial T}{\partial z} = 0 \tag{A.46}$$

hence

$$e = \lambda_{13} . \tag{A.47}$$

The isothermal electric conductivity is,

$$\sigma_e = J_r / -E_r = -J_r / E_r \tag{A.48}$$

$$\frac{\partial T}{\partial r} = \frac{\partial T}{\partial z} = J_z = 0 , \tag{A.49}$$

hence

$$\sigma_e = 1/\lambda_{11} .$$

The isothermal heat conductivity is,

$$k = q_r / \frac{\partial T}{\partial r} , \quad \text{when} \quad J_r = J_z = \frac{\partial T}{\partial z} = 0 \tag{A.50}$$

hence

$$k = \lambda_{33} . \tag{A.51}$$

The isothermal Hall effect is defined as,

$$R_H = -E_z / BJ_r , \quad \text{if} \quad J_z = \frac{\partial T}{\partial r} = \frac{\partial T}{\partial z} = 0 \tag{A.52}$$

hence $$R_H = \lambda_{12}/B \ . \qquad (A.53)$$

The isothermal Nernst-Ettinghausen effect is,

$$A_{ne} = E_z/B \frac{\partial T}{\partial r} , \quad \text{when} \quad \frac{\partial T}{\partial z} = J_r = J_z = 0 \qquad (A.54)$$

hence (6):

$$A_{ne} = \lambda_{14}/B \qquad (A.55)$$

and the Leduc-Righi effect is,

$$L = \frac{\partial T}{\partial z}/B \frac{\partial T}{\partial r} , \quad \text{if} \quad q_z = J_z = J_r = 0 \qquad (A.56)$$

hence

$$L = \lambda_{34}/\lambda_{33} \ B \ . \qquad (A.57)$$

It should be noted that the last three descriptive coefficients are functions of the magnetic field. Applying the descriptive coefficients to (A.44) gives the conventional matrix set as shown by Callen (30).

$$\begin{pmatrix} E_r \\ E_z \\ q_r \\ q_z \end{pmatrix} = \begin{pmatrix} \sigma_e^{-1} & R_H B & -e & -A_{ne} B \\ -R_H B & \sigma_e^{-1} & A_{ne} B & -e \\ -eT & -A_{ne} BT & -k & -kBL \\ A_{ne} BT & -eT & kBL & -k \end{pmatrix} \cdot \begin{pmatrix} J_r \\ J_z \\ \frac{\partial T}{\partial r} \\ \frac{\partial T}{\partial z} \end{pmatrix} \qquad (A.58)$$

Equation (A.58) is referred to by Callen as the fundamental set of dynamical equations for the direct current problem. This result is in complete agreement since the quantities contributing to the matrix set from polarization phenomena have been shown to be negligible in the case of bismuth at low frequencies, 60 cps. Therefore, the alternating current magnetothermoelectric equations reduce to the direct current case.

APPENDIX B

DERIVATION OF EDDY CURRENT RELATIONS

If there is relative motion between a magnetic field and a metallic conductor, then an induced current is established. These induced currents are, in general, disadvantageous and efforts are usually taken to minimize their production. The transformer industry is probably foremost in developing techniques for the reduction of these currents. The chief method recommended is to use thin layers, usually laminated, or either many separate conductors.

In the particular problem considered, the thickness is small but the eddy current will be shown to be significant. Hence it is desired to compute the local eddy current, the zero eddy current radius, r_m, and derive an expression for the power dissipated. Re-examining Figure 4.

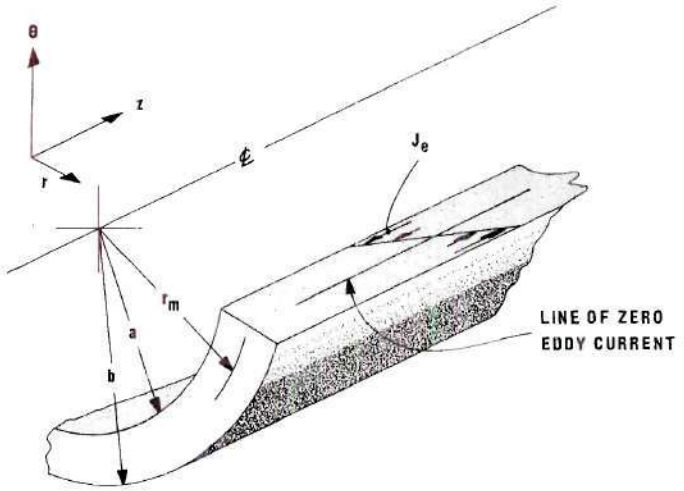

Figure 4. Eddy Currents

The assumption of infinite length in the longitudinal direction allows once again neglecting any end effects.

Recall from Appendix A Maxwell's fourth equation

$$\nabla \times \bar{E} = - \frac{\partial \bar{B}}{\partial t} \qquad (A.10)$$

where B is given by the expression

$$\bar{B}\Big|_{\theta} = C_o(1/r) = -2I(10^{-7}) \frac{\sin (\omega t)}{r} \quad . \qquad (2.3)$$

Substitution of (2.3) into (A.10) yields

$$\frac{\partial E_r}{\partial z} - \frac{\partial E_z}{\partial r}\Big|_{\theta} = 240\pi \cdot 10^{-7} (\frac{I}{r}) \sin \omega t \ ; \qquad (B.1)$$

since the first derivative is zero. Thus

$$\frac{\partial E_z}{\partial r} = \frac{dE_z}{dr} = -240\pi \cdot 10^{-7}(\frac{I}{r}) \quad . \qquad (B.2)$$

This may be shown as follows:

Writing the curl of the electric field:

$$\left[\frac{1}{r}\frac{\partial E_z}{\partial \theta} - \frac{\partial E_\theta}{\partial z}\right]_r + \left[\frac{\partial E_r}{\partial z} - \frac{\partial E_z}{\partial r}\right]_\theta + \tag{B.3}$$

$$\left[\frac{1}{r}\frac{\partial}{\partial r}(r\,E_\theta) - \frac{1}{r}\frac{\partial E_r}{\partial \theta}\right]_z = -\frac{\partial B_\theta}{\partial t}$$

The magnetic field is only in the angular direction, i.e.,

$$\bar{B} = 0\,\bar{r} + B_\theta\,\bar{\theta} + 0\,\bar{k}\ . \tag{B.4}$$

Equating the components and applying the infinite length conditions:

$$\left[\frac{1}{r}\frac{\partial E_z}{\partial \theta} - \frac{\partial E_\theta}{\partial z} = 0\right]_r \tag{B.5}$$

$$\left[\frac{\partial E_r}{\partial z} - \frac{\partial E_z}{\partial r} = -\frac{\partial B_\theta}{\partial t}\right]_\theta$$

$$\left[\frac{1}{r}\frac{\partial}{\partial r}(rE_\theta) - \frac{1}{r}\frac{\partial E_r}{\partial \theta} = 0\right]_z$$

The condition of infinite length eliminates the following terms:

$$\frac{\partial E_\theta}{\partial z} = \frac{\partial E_r}{\partial z} = 0 \tag{B.6}$$

Hence:

$$\frac{1}{r}\frac{\partial E_z}{\partial \theta} = 0 \tag{B.7}$$

$$\frac{-\partial E_z}{\partial r} = \frac{-\partial B_\theta}{\partial t} \qquad (B.8)$$

and the requirement of azimuthal symmetry gives:

$$\frac{\partial E_r}{\partial \theta} = 0 \ .$$

Therefore the differential equation is

$$\frac{\partial}{\partial r}(r\, E_\theta) = 0 \quad . \qquad (B.9)$$

Integration of Equation (B.7) gives the expected result

$$E_z = \text{constant} \ . \qquad (B.10)$$

Integrating Equation (B.8) yields,

$$E_z = \int \frac{\partial B}{\partial t}\, dr \ . \qquad (B.11)$$

Equation (B-9) may be also integrated to find

$$E = \text{Const}/r \qquad (B.12)$$

where the constant is found to be zero from symmetry considerations. Thus the entire set of Equations (B.5) reduces to the equation

$$E_z = \int \frac{\partial B}{\partial t}\, dr \qquad (B.11)$$

Recalling the expression for the magnetic field, Equation (2.1), after first performing the differentiation:

$$E_z = \int -2I\ 10^{-7}\ \frac{\omega \sin \omega t}{r}\ dr \qquad (B.13)$$

Integrating gives:

$$E_z = [-2\ I\ 10^{-7}\ \omega \sin \omega t]\ln(r) + C_3$$

where $\omega = 2\pi f = 120\pi$ and C_3 is a constant of integration.

$$E_z = -240\pi\ 10^{-7}\ I(\ln r) + C_3 \qquad (B.14)$$

The constant C_3 is easily determined since $E_z = 0$ at radius r_m.

Hence,

$$E_z = (-240\pi\ 10^{-7}\ I)\ln(r/rm) \qquad (B.15)$$

Applying Ohm's law in the simplest form,

$$J_e = E_z/\rho_r \qquad (B.16)$$

and using Equation (B.5),

$$0 = \int_a^b J_e \, r dr d\theta = \frac{2\pi}{\rho_r} \int_a^b E_{ze} \, r dr = \tag{B.17}$$

$$2\pi^2(-240)\ 10^{-7}\ \frac{I}{\rho_r} \int_a^b \mathrm{Ln}(r/r_m)\ r dr$$

Dividing out the constant,

$$\int_a^b \mathrm{Ln}(r/r_m)\ r dr = 0 \tag{B.18}$$

It is seen that the location of the zero eddy current line is independent of any parameter except the radius, or rather the difference between the internal and external radii. Solving (B.7) for r_m when a = 0.50 and b = 1.00 gives

$$r_m = 0.764 \tag{B.19}$$

Then rewriting Equation (B.5)

$$J_e = [-240\ \pi^2\ 10^{-7}\ I/\rho_r](\mathrm{Ln}\ r/r_m) = G\ I[\ell n\ (\frac{r}{r_m})] \tag{B.20}$$

Using the nominal value of the resistivity, ρ_r, for bismuth at room temperature.

$$\rho_r = 11.9 \times 10^{-7}\ \text{ohm-m} \tag{B.21}$$

A simple expression for the eddy current is obtained.

$$J_e = \frac{-240\pi^2\ 10^{-7}}{\rho_r} [I\ Ln(r/r_m)] \tag{B.22}$$

$$J_e = -63.2[I\ Ln(r/r_m)] \tag{B.23}$$

The last of the objectives of this Appendix is to determine the expression for the dissipation of power from the eddy currents that are developed. The local power is

$$P_e = \int_{vol} \rho(J_e)^2\ dVol \tag{B.24}$$

Using the expression for the elemental volume, the average power per unit volume per unit length is found.

$$\overline{Pe} = 2\pi\ \rho_r \int_{r=a}^{r=b} J_e^2\ rdr\ . \tag{B.25}$$

Appendix C
Computer Program

```
          BEGIN
%         WALL, DONALD B. MECHANICAL ENGINEERING, THE TEMPERATURE PROFILE
%         FOR A NERNST-ETTINGHAUSEN HEAT PUMP IS SOLVED BY THE RUNGE-
%         KUTTA METHOD. THIS NUMERICAL METHOD REQUIRES KNOWLEDGE OF THE
%         FIRST DERIVATIVE AT THE INSIDE BOUNDARY. THIS DERIVATIVE WAS
%         FOUND FOR EACH J AND T BY ASSUMING A DERIVATIVE, ITERATING, AND
%         THEN EXAMINING THE FUNCTION AT THE OUTER BOUNDARY. IF THE VALUE
%         OF THE FUNCTION IS NOT AS DESIRED AN ADJUSTMENT IS MADE IN THE
%         BOUNDARY CONDITIONS TEST ROUNTINE TO THE INITIAL DERIVATIVE
%         UNTIL THE DESIRED FUNCTION IS OBTAINED. THE INITIAL DERIVATIVES
%         SHOWN IN THE SECTION ENTITLED INITIAL DERIVATIVES WERE FOUND
%         IN THIS MANNER.
INTEGER   M,N                                                          ;
REAL      XI,XO,YI,YO,RI,RO,AREA,L,JA,J,ALFHA,BETA,TIN,TOUT,G,RHO,
          ANE,XM,HI,LO,DX,TM,H,I,JAP,C,KT,DYI,X1,X2,K1,K2,K3,DK1,DK2,
          DK3,Y1,Y2,DY1,DY2,YOUT,QNERNST,QCON,QTOTAL,EMF,MAG,JEDDY,
          QINSIDE,QOUTSIDE,COP,TB,TT,GAMA,SLOPE,EMFIN,EMFOUT,Z,W,QNEREDD;
ARRAY           X,Y,DY,DDYI0:1022]                                     ;
FILE OUT  DRW 6(2,15)                                                  ;
LABEL     L3,L5,L6,B1,B2,B3,B4                                         ;
LIST      ANS2(X[M],((Y[M]*TOUT-TIN)/(TOUT-TIN)),DY[M],DDY[M],Y[M]*TOUT,
EMF)      ;
LIST      ANS3(X[M],QNERNST*6.28*X[M]*RO*L,QCON*6.28*X[M]*RO*L,QTOTAL,
MAG,QNEREDD)                ;
LIST      ANS4(COP)                                                    ;
LIST      ANS(I,JA)                                                    ;
FORMAT    FMT(/X9,"THE MAGNETIC CURRENT IS",F15.2,X5,"AMPS AND THE WORKIN
G ELECTRON CURRENT IS",F10.2,X3,"AMPERES"//)                           ;
FORMAT    FMT1(/X8,"X",X12,"Y",X11,"DY",X11,"DDY",X10,"TEMP",X13,"EMF",
X2,/)                                                                  ;
FORMAT    FMT2(/6F13.4/)                                               ;
FORMAT    FMT3(/6F15.4/)                                               ;

FORMAT    FMT4(//"THE C.O.P IS",F10.5//)                               ;
FORMAT    FMT5(//X9,"X",X9,"QNERNST",X9,"QCON",X9,"QTOTAL",X9,"MAG FIELD",
          X4,"EDDY(QNERNST)"//)                                        ;
          WRITE(DBW[NO])                                               ;
```

Appendix C
(continued)

```
%                          INITIAL INPUT DATA


        EMFIN  ←  0.8150                                                ;
        EMFOUT ←  0.915                                                 ;
        TIN ← (25.4×EMFIN)+ 273.0                                       ;
        TOUT ←  ( 25.4×EMFOUT) + 273.0                                  ;


%                          VARIABLE PARAMETERS

        FOR JA ← 0,500,1000,2000              DO
        BEGIN
        N ← -2                                                          ;
L6:     N  ← N + 2                                                      ;
        I ← N×1600.0                                                    ;

%                          INITIAL VALUES

        YI ← (TIN/TOUT)                 ;       YOUT ← 1.0              ;
        RO ← 0.0254                     ;       AREA ← 0.001520         ;
        G  ← 53.2×I                     ;       XM ← 0.7640             ;
        C  ←   2.0@-7                   ;       KT ← 8.10               ;
        RI  ← 0.50 × RO                 ;       L ← 3.0×0.0254          ;
        DX  ←  0.50/1000                ;       JAP ←  JA/AREA          ;

        XO ←  1.0                       ;       RHO ← 11.9@-7           ;
        ANE ← -0.8@-3                   ;       XI ←  0.50              ;
        ALFHA ←(2.0×(JAP)×C×I×ANE)/KT                                   ;
        BETA ← (2.0×G×C×I×ANE)/KT                                       ;
        GAMA ← (RO*2)×RHO/(TOUT×KT)                                     ;
```

Appendix C
(continued)

```
                        INITIAL  DERIVATIVES

          IF JA= 0          THEN GO TO B1                    ;
          IF JA= 500        THEN GO TO B2                    ;
          IF JA= 1000       THEN GO TO B3                    ;
          IF JA= 2000       THEN GO TO B4                    ;
B1:       IF I =   0      THEN  DYI ← 0.02490                ;
          IF I =   3200   THEN  DYI ← 0.01611                ;
          IF I =   6400   THEN  DYI ←-0.00977                ;
          IF I =   9600   THEN  DYI ←-0.052730               ;
        GO TO L5    ;
B2:       IF I =   0      THEN  DYI ← 0.03467                ;
          IF I =   3200   THEN  DYI ← 0.024410               ;
          IF I =   6400   THEN  DYI ←-0.003420               ;
          IF I =   9600   THEN  DYI ←-0.047850               ;
        GO TO L5    ;
B3:       IF I =   0      THEN  DYI ← 0.06484                ;
          IF I =   3200   THEN  DYI ← 0.05195                ;
          IF I =   6400   THEN  DYI ← 0.02227                ;
          IF I =   9600   THEN  DYI ←-0.023830               ;
        GO TO L5    ;
B4:       IF I =   0      THEN  DYI ← 0.18604                ;
          IF I =   3200   THEN  DYI ← 0.165500               ;
          IF I =   6400   THEN  DYI ← 0.12988                ;
          IF I =   9600   THEN  DYI ← 0.078610               ;
```

Appendix C
(continued)

```
%                          INITIALING THE ARRAY

L5:     X[0] ← XI    ;   Y[0] ← YI ;       DY[0] ← DYI                    ;
        DDY[0] ←(-DY[0]×(ALFHA+BETA×LN(X[0]/XM)+1)×(1.0/X[0]))-(Y[0]×(
        0.50×BETA)×(1.0/(X[0]↑2)))-(GAMA×((JAP)+G×LN(X[0]/XM))↑2)       ;

%                          MAIN PROGRAM

        FOR M ← 0  STEP 1 UNTIL 999    DO
BEGIN
        H ← DX                                                          ;
        X[M+1]  ←  X[0] + (M+1)×DX                                      ;
        K1 ← (H×DY[M])                                                  ;
        DK1 ← (H×DDY[M])                                                ;
        X1  ←  X[M] +  0.50×H                                           ;
        Y1  ←  Y[M] + 0.50×K1                                           ;
        DY1  ←  DY[M] + 0.50×DK1                                        ;
        K2  ←  H× (DY1)                                                 ;
        DK2←H×((-DY1×(ALFHA+BETA×LN(X1/XM)+1)×(1.0/X1))-(Y1×(0.50×BETA)
        ×(1.0/(X1↑2)))-(GAMA×(JAP  +  G× LN(X1/XM))↑2))                 ;
        X2 ← X[M] +H                                                    ;
        Y2 ← Y[M] + 2.0×K2 - K1                                         ;
        DY2  ←  DY[M] + 2.0×DK2 - DK1                                   ;
        K3 ← H×(DY2)                                                    ;
        DK3 ←H×((-DY2×(ALFHA+BETA×LN(X2/XM)+1.0)×(1.0/X2))-(Y2×(0.5
        ×BETA)×(1.0/(X2↑2)))-(GAMA×(JAP + G×LN(X2/XM))↑2))              ;
        Y[M+1]  ← Y[M]  +  ((K1 + 4.0×K2 + K3)/6.0)                     ;
        DY[M+1]  ← DY[M]  +  ((DK1 + 4.0×DK2 + DK3)/6.0)                ;
        DDY[M+1] ← (-DY[M+1]×(ALFHA + BETA×LN(X[M+1]/XM)+1.0)×(1.0/X[
        M+1]))-(Y[M+1]×(0.50×BETA)×(1.0/(X[M+1]↑2))) - (GAMA×(JAP +
        G×LN(X[M+1]/XM))↑2)                                             ;
END                                                                     ;
```

Appendix C
(continued)

```
%                              BOUNDARY CONDITIONS TEST
%       HI ← 10.00       ;     LO ← -10.00                                    ;
%       IF (Y[1000]-YOUT)  <  -0.0001     THEN GO TO L1                       ;
%       IF (Y[1000]-YOUT)  <   0.0001     THEN GO TO L2                       ;
%       GO TO L3                                                              ;
%L2:    HI ←  DYI             ;     GO TO L4                                  ;
%L1:    LO ←  DYI             ;     GO TO L4                                  ;
%       DYI ← ( HI + LO)×0.50          ;   GO TO L5                           ;

%                              PRINT OUT

L3:     WRITE(DBW,FMT,ANS)                                                    ;
        WRITE(DBW,FMT1)                                                       ;
        FOR M ← 0  STEP  20  UNTIL  1000       DO
%                              TEMPERATURE PROFILE
BEGIN
        EMF ← (((Y[M]×TOUT)-273.0)/(25.400))                                  ;
        WRITE(DBW,FMT2,ANS2)             ;      END                           ;
        WRITE(DBW,FMT5)                                                       ;
        FOR M ← 0  STEP  200 UNTIL  1000       DO
BEGIN
        MAG   ←  C×I/(RO×X[M])                                                ;
        QNERNST  ← -MAG×ANE×(JAP+G×LN(X[M]/XM))×Y[M]×TOUT                     ;
        QCON  ←  - KT×DY[M]×TOUT/RO                                           ;
        QTOTAL  ←  QCON  +  QNERNST                                           ;
        QNEREDD ← -MAG×ANE×G×LN(X[M]/XM)×Y[M]×TOUT                            ;
        IF M = 0       THEN QINSIDE  ← QTOTAL                                 ;
        IF M =  1000       THEN  QOUTSIDE ← QTOTAL                            ;
        WRITE(DBW,FMT3,ANS3)          ;        END                            ;
        IF QOUTSIDE × QINSIDE > 0.00       THEN
```

Appendix C
(continued)

```
BEGIN

        Z ← @INSIDE×(RI)                                        ;
        W ← @OUTSIDE×(RO)                                       ;
        IF Z >   0.0        THEN
        COP ← 1.0/(1-(Z/W))
ELSE    COP ← 1.0/(1-(W/Z))                                     ;
END
ELSE        COP ←   999.666 !& THIS OUTPUT IS INVALID COP
        WRITE(DBW,FMTA,ANSA)                                    ;

      IF N <   6     THEN GO TO LA                              ;
END!                                  END.
```

APPENDIX D

ERROR ANALYSIS

Selecting a method for any temperature measurements requires numerical understanding of the required degree of precision. It is a fundamental truth that all measurements are merely imperfect attempts to determine an exact natural state of condition. The actual value of the desired quantity will never be known. Hence, the actual error between the real value and the observed value should be discussed only in terms of probabilities. That is, the error probably is correct to within a certain specification (36).

The error resulting from reading instruments, small disturbances, or fluctuating conditions are small and classified as random errors. It is estimated that the total random error is less than 5 per cent. There are four main sources of systematic error in this experimental apparatus. The largest of these should be the known location of the temperature sensing plane of the thermocouple bead. The dimension of the test sample in the radial direction is one-half inch and within this space, six thermocouples are placed. Each thermocouple bead is 0.020 inches in diameter. This single fact alone shows that approximately 20 per cent of the radius is thermocouple material. The exterior thermocouples, TC 1 and 6, are placed on the inside of the test specimen and consequently do not indicate the surface temperature but rather the temperature near the surface. It is estimated that the

location of these thermocouples is 0.040 inches, two bead diameters, from the surface. The other thermocouples are evenly distributed. It was desired to place the thermocouples as the following radii:

TC1	located at	0.540 radius
TC2	located at	0.600 radius
TC3	located at	0.700 radius
TC4	located at	0.800 radius
TC5	located at	0.900 radius
TC6	located at	0.960 radius

The thermocouples were aligned initially in the mold by placing them on a polar grid between the break-a-way sections of the mold, next tightening down the mold, and then removing the grid. The bismuth metal was then melted and poured around the thermocouples. It may be expected that some movement of the thermocouples occurred during the casting process, however, the error in the initial placement and as a result of any movement afterwards is considered less than 10 per cent. In this regard an error calculation is performed using a 10 per cent variation in location.

The second largest error is the result of the insertion of the thermocouple within the test specimen. As was mentioned above, the thermocouples occupy approximately 20 per cent of a radial line drawn from the interior to the outer surface. In order to analyze this effect--the insertion of foreign material within the test specimen--an analytical model which represents at least the largest error is developed. As before, the longitudinal and azimuthal heat fluxes are zero.

Consider, in place of a thermocouple, a shell of thickness equal to the bead thickness (0.020 inch) is placed at the thermocouple locations. The shell is constructed of copper which has essentially the same properties as copper-constantan junction. This is acceptable since the properties of copper are further removed from the properties of bismuth than the material constantan. A cross section of the analytical model is given in Figure 21.

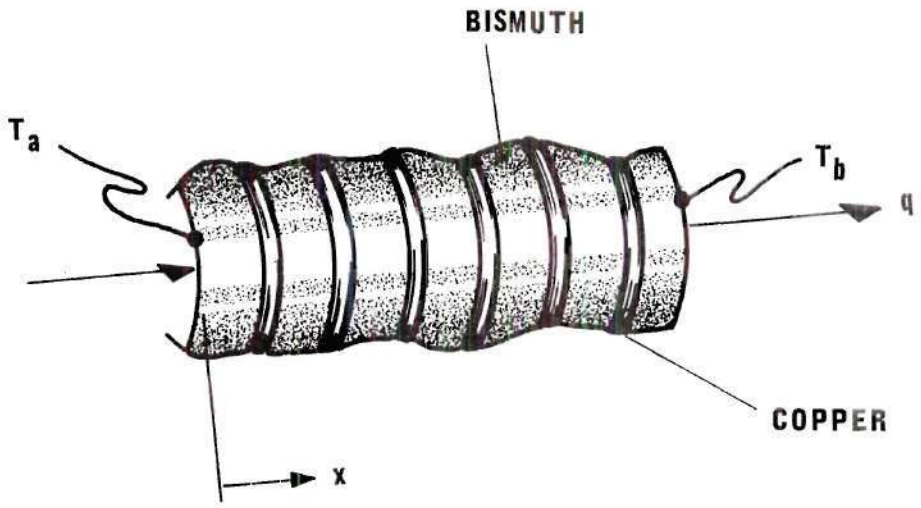

Figure 21. Analytical Model Used in the Error Analysis

The surface temperatures, T_a and T_b, are the same as considered in the analytical investigation. The radius of each shell is identical to the radial distance of the thermocouples. The problem thus resolves to a mathematical treatment of this "sandwich" construction and then to compare the resulting temperature profile with the pure bismuth profile. The difference between the two profiles indicates

the amount of error introduced by the presence of the thermocouple material.

It is apparent the differential equation, (2.13), will remain the same with the only adjustment being the changes in the properties of the material. The magnetothermoelectric properties, except the thermal conductivity and the electrical resistivity, are considered zero for the copper material.

The differential equation for the copper shells is

$$\frac{d^2Y'}{dX^2} + \frac{1}{X}\frac{dY'}{dX} + \frac{\rho_{cu}}{T_b}\frac{b^2J^2}{k_{cu}} = 0 \qquad (D.1)$$

Both Equations (D.1) and (2.13) therefore must be used together to calculate the temperature profile for the "sandwich" construction. The initial computer program was modified to include this adjustment. The program was developed to integrate Equation (2.13) from the inner radius out to the first shell located at x = .540. From this location out to x = 0.560, the copper Equation, (D.1), was applied. At x = 0.560 the bismuth Equation (2.13) was then reapplied and this process was continued out to the exterior surface, x = 1.00. The difference in the bismuth and bismuth-copper temperature profiles is shown in Figure 22. The percentage error given for x = 0.800 is seen to be less than 4 per cent.

The other main contributors to the total error is the accuracy of the electrical current measuring devices. The ammeters used for measuring both the working electrical current, J, and the magnetizing

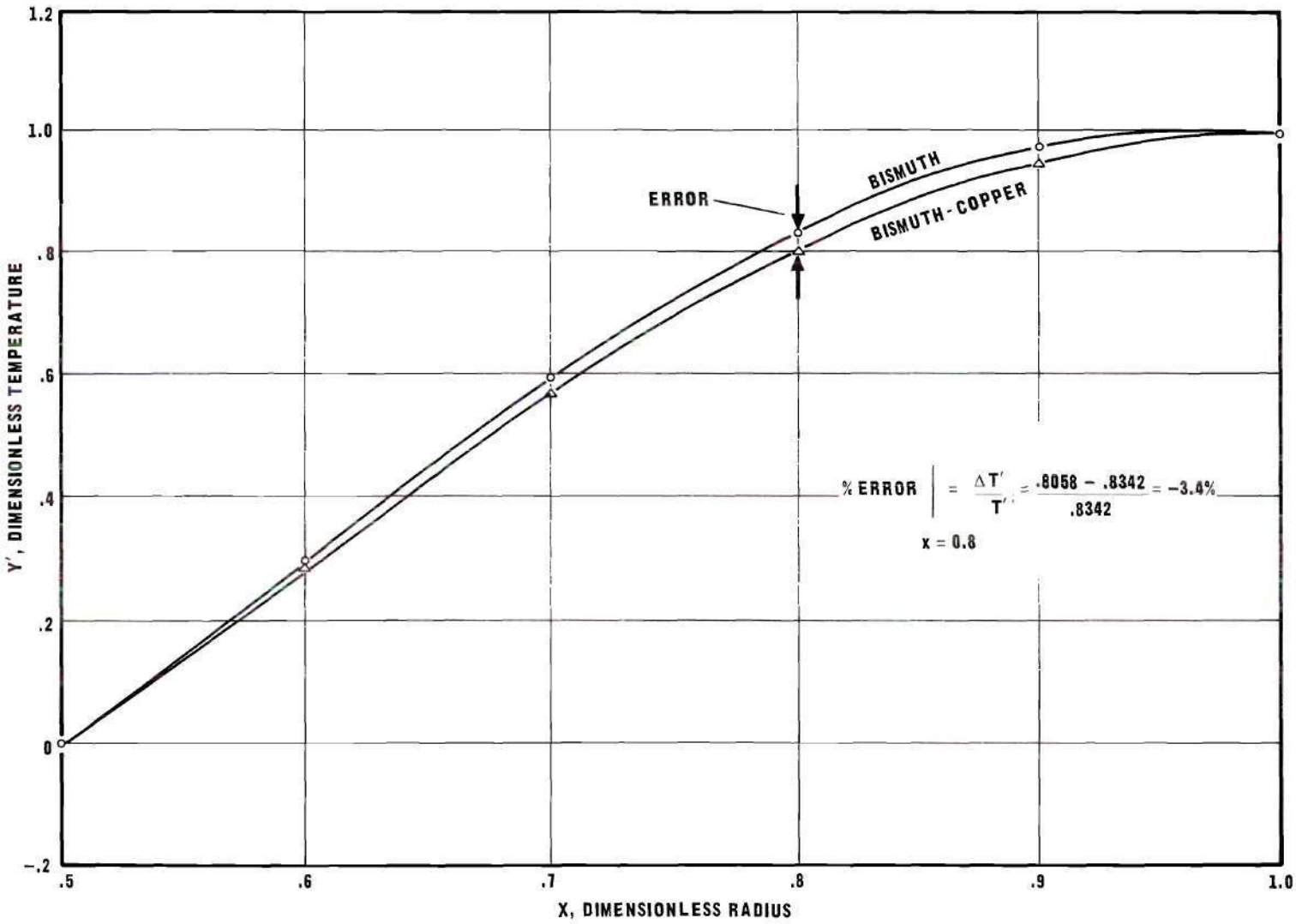

Figure 22. Comparison of Bismuth and Bismuth-Copper Temperature Profiles.

current, I, were stated to be within 5 per cent accuracy for full scale deflection. Therefore, it is reasonable to assume that the error in either J or I is approximately 5 per cent since the observed values were near full scale deflection.

A functional relationship is derived for the maximum systematic error which may be present. This error can be expressed as

$$\text{Error} = \text{Error}\ (J,I,x) \quad \text{and} \quad \text{Error}\ (\text{Copper-Bismuth}).$$

That is, the error which can be expected is composed of two error sources. The first group contains the error of those quantities which are measured. The second group is the error introduced from the insertion of the copper-constantan thermocouples.

Since the calculated error will be different for different values of the parameters, the particular situation of maximum current used in the experimental tests, for both J and I and a location of $x = 0.800$, is taken as an example.

The amount of the working electric current, is 1000 amps; therefore, the variation ΔJ, due to instrument accuracy of 5 per cent is ± 50 amps--a spread of 100 amps. Similarly, for the magnetizing current of 6400 amps, a 5 per cent variation ΔI, is ± 320 amps.

The error due to the measured quantities can be expressed in a functional relationship as

$$\text{Per cent error} = \frac{dY'}{Y'} = \frac{1}{Y'}\left[\frac{\partial Y'}{\partial I}\,dI + \frac{\partial Y'}{\partial J}\,dJ + \frac{\partial Y'}{\partial X}\,d\dot{x}\right] \qquad (D.2)$$

where the non-dimensional temperature, Y', is expressed as

$$Y' = Y'(I,J,x) \tag{D.3}$$

Replacing the partial derivative equation by the approximate finite difference equation,

$$\text{Per Cent Error} = \frac{\Delta Y'}{Y} = \frac{1}{Y'}\left[\frac{\Delta Y'}{\Delta I}\Delta I + \frac{\Delta Y'}{\Delta J}\Delta J + \frac{\Delta Y'}{\Delta X}\Delta X\right] \tag{D.4}$$

The first coefficient, $\Delta Y'/\Delta I$, which is considered at J = 1000 amps and x = 0.800, is computed from the computer program. This coefficient is

$$\frac{1}{Y'}\left(\frac{\Delta Y'}{\Delta I}\right) = \frac{.8726 - .8076}{.8342 \quad (640)} = 1.2 \times 10^{-4} \text{ amp}^{-1}$$

The second coefficient, $\frac{1}{Y'}\left(\frac{\Delta Y'}{\Delta J}\right)$, is also taken at I = 6400 amps and x = 0.800.

$$\frac{1}{Y'}\left(\frac{\Delta Y'}{\Delta J}\right) = \frac{.8836 - .7902}{.8342 \quad (100)} = 9.34 \times 10^{-4} \text{ amp}^{-1}$$

The third coefficient, $\frac{1}{Y'}\left(\frac{\Delta Y'}{\Delta x}\right)$, is

$$\frac{1}{Y'}\left(\frac{\Delta Y'}{\Delta x}\right) = \frac{.8538 - .8137}{.8342 \quad (.010)} = 4835 \text{ inch}^{-1}$$

Placing the above coefficients into the error equation, (D.4), gives,

$$\text{Error } (J,I,x) = 1.2 \times 10^{-4} (640) + 9.34 \times 10^{-4} (100) \quad (D.5)$$

$$+ 4.85 (0.010) = 19.99 \times 10^{-2}$$

The probable error from observing the measured electric currents, I and J, and of measuring the exact location of each thermocouple is less than ±11 per cent. The total error obtained from both error sources is

$$\text{Total error} = \pm 11\% - 3.4\% = -14.4\% \text{ or } + 7.6\%$$

The error caused by the insertion of the thermocouples is negative. This makes the error band asymmetrical. An error of +7.6 per cent and a larger error of -14.4 per cent is probable. The error band is plotted in Figures 17 and 18. These graphs give the analytical curves, the error band, and the actual measured data points. The data points all fall within the maximum error band.

APPENDIX E

EQUIPMENT LIST

T1	Transformer, current General Electric Type JCD-0,8000/5
T2	Powerstat, variable transformer Superior Electric Co. 20amp-240v
T3, T4	Transformer, 10:1 Westinghouse S10n05S07D, 7 1/2 KVA
T5	Transformer, variable General Electric Volt-pac-SN9H95MF50X, 0-240 amps, 0-240 volt
T6, A2	Current Transformer, ammeter General Electric clip-on type 0-600 amps
A1	Ammeter General Electric 0-10 amps ac
Pot	Potentiometer Leeds & Northrup Type K3
Galv	Galvanometer Leeds & Northrup Light type Cat. 2430-A
TC	Thermocouples, copper-constantan, 0.008 inch Omega Engineering, Inc.

APPENDIX F

SPECTROGRAPHIC ANALYSIS OF TEST SPECIMEN

A spectrographic analysis of the bismuth specimen showed the above constituents (by percentage):*

Antimony		0.007
Copper		0.001
Silver		0.002
Zinc		0.003
Iron		0.001
Lead		0.002
Arsenic	less than	0.001
Bismuth		99.983+

*MacMillan Laboratories, Atlanta, Georgia.

APPENDIX G

PROPERTIES

The following properties used in this investigation are taken from the references indicated.

$$\rho_{r_{Bi}} = 1.18 \times 10^{-8} \text{ ohm-m} \quad (27)$$

$$k_{Bi} = 8.1 \text{ Watts/}^{\circ}\text{K m}^2 \quad (27)$$

$$A_{ne_{Bi}} = 0.8 \times 10^{-3} \ ^{\circ}\text{K m}^2\text{/sec} \quad (20)$$

$$\rho_{cu} = 1.7\ 24 \times 10^{-8} \text{ ohm-m} \quad (37)$$

$$k_{cu} = 386 \text{ watt/}^{\circ}\text{K m}^2 \quad (37)$$

BIBLIOGRAPHY

REFERENCES CITED

1. B. Varga, A. D. Reich and J. R. Madigan, "Thermoelectric and Thermomagnetic Heat Pumps," *Journal of Applied Physics*, v. 34, n. 12, December, 1963.

2. A. F. Ioffe, "The Revival of Thermoelectricity," *Scientific American*, v. 199, n. 5, November, 1958, p. 31.

3. G. Shortley and D. Williams, *Physics*, Prentice-Hall, Inc., Englewood Cliffs, N. J., 1962.

4. H. J. Goldsmid, "Thermoelectric and Thermomagnetic Cooling," *Industrial Electronics*, May, 1963, p. 441.

5. R. Wolfe and G. E. Smith, Physics of Thermoelectricity, and Thermoelectric Materials," *Bell Telephone System Monograph*, 45183, 1963.

6. Allen Nussbaum, *Semiconductor Device Physics*, Prentice-Hall, Inc., Englewood Cliffs, N. J., 1962.

7. R. T. Delves, "The Prospects for Ettinghausen and Peltier Cooling at Low Temperatures," *British Journal of Applied Physics*, v. 13, 1962.

8. P. W. Bridgman, *The Thermodynamics of Electrical Phenomena in Metals*, The MacMillan Co., New York, 1934.

9. Edwin J. Scheibner, "Solid-State Physical Phenomena and Effects," Georgia Institute of Technology, Engineering Experiment Station, Spec. Report 40, 1963.

10. B. J. O'Brien and C. S. Wallace, "Ettinghausen Effect and Thermomagnetic Cooling," *Journal of Applied Physics*, v. 29, n. 7, July, 1958, p. 1010.

11. T. C. Harman and J. M. Honig, "Theory of Galvano Thermomagnetic Energy Conversion Devices II, Refrigerators and Heat Pumps," *Journal of Applied Physics*, v. 33, n. 11, November, 1963, pp. 3188.

12. M. R. El-Saden, "Theory of the Ettinghausen Cooler," *Journal of Applied Physics*, v. 33, n. 3, May, 1961.

13. T. O. Harman and J. M. Honig, "Nernst-Ettinghausen (Transverse) Energy Conversion," *Semiconductor Products*, July, 1963, p. 19.

14. B. V. Paranjape and J. S. Levinger, "Theory of the Ettinghausen Effect in Semiconductors," *Physical Revue*, v. 120, n. 2, October, 1960.

15. R. B. Horst, "Thermomagnetic Figure of Merit: Bismuth," *Journal of Applied Physics*, v. 34, n. 11, November, 1963.

16. S. W. Angrist, "A Nernst Effect Power Generator," *Journal of Heat Transfer*, February, 1963.

17. T. O. Harman, et al., "Experiments on Room Temperature Nernst-Ettinghausen Refrigerators," SAE Paper 842A, 27, April, 1964.

18. Robert L. Sproull, *Modern Physics*, John Wiley & Sons, Inc., New York, N. Y., 2nd Edition, 1963.

19. Raymond Wolfe, "Magnetothermoelectricity," *Scientific American*, June, 1964.

20. T. C. Harman and J. M. Honig, "Nernst and Seebeck Coefficient in Bismuth at High Magnetic Fields," *Advanced Energy Conversion*, v. 3, p. 525, 1963.

21. R. Wolfe and G. E. Smith, "Effects of a magnetic field of the thermoelectric properties of bismuth-antimony alloys," *The Physics of Semiconductors*, The Institute of Physics and the Physics Society, London, 1962.

22. P. Mazure and S. R. DeGroot, *Non-Equilibrium Thermodynamics*, North-Holland Pub. Co., Amsterdam, 1962.

23. F. B. Hildebrand, *Advanced Calculus for Engineers*, Prentice-Hall, Inc., Englewood Cliffs, N. J., 1948.

24. M. W. Zemansky, *Heat and Thermodynamics*, McGraw-Hill Book Company, New York, 4th Edition, 1957.

25. International Critical Tables, McGraw Hill Co., New York, v. 6, p. 420, 1928.

26. G. E. Smith and R. Wolfe, "Thermoelectric Properties of Bismuth-Antimony Alloys," *J. Applied Physics*, v. 33, pp. 841-846, March, 1962.

27. Smithsonian Physical Tables, 9th Edition, 1956, Washington, D. C., Table 134.

28. G. Smith Hopkins and J. O. Bailar, Jr., *General Chemistry for Colleges*, 5th Edition, D. C. Heath and Co., Boston, Mass., 1956.

29. *Radiography in Modern Industry,* 2nd Edition, Eastman Kodak Co., Rochester 4, N. Y., 1957.

30. H. B. Callen, *Thermodynamics,* John Wiley and Sons, Inc., New York, 1964.

31. Gordon J. Van Wylen, *Thermodynamics,* John Wiley and Sons, Inc., New York, 1964.

32. S. R. Degroot, *Thermodynamics of Irreversible Processes,* North-Holland Publishing Co., Amsterdam, 1951.

33. I. Prigogine, *Introduction to Thermodynamics of Irreversible Processes,* Charles C. Thomas, Springfield, Ill., 2nd Edition, 1961.

34. C. R. Wylie, Jr., *Advanced Engineering Mathematics,* McGraw Hill Book Co., New York, 1951.

35. J. P. Jan, "Galvanomagnetic and Thermomagnetic Effects in Metals," *Solid State Physics,* v. 5, 1957.

36. Yardley Beers, *Theory of Error,* Addison-Wesley Publishing Co., Inc., Reading, Mass., 1957.

37. *Mechanical Engineers Hand Book,* McGraw Hill Book Company, Inc., New York, N. Y., Sixth Edition, 1958.

References Not Cited

S. W. Angrist, "On the Boundedness of the Dimensionless Index of Performance on a Nernst Effect Generator," *Journal of Applied Mechanics,* June, 1963, p. 261.

J. F. Elliott, "Thermomagnetic Generator," *Journal of Applied Physics,* Vol. 30, Number 11, p. 1774, November, 1959.

E. Englert and K. Schuster (Munchen), "Die Magnetiche Widerstandsanderung eines Wismutdrahtees," *Physik, Seitscher,* XXXIV, 1933.

W. G. Evans, "Characteristics of Thermoelectric Materials," *Semiconductor Products,* p. 34, April, 1963.

T. C. Herman and J. M. Honig, "Theory of Galvano-Thermomagnetic Energy Conversion Devices, I, Generators," *J. of Applied Physics,* v. 33, n. 11, November, 1963, p. 3178.

A. F. Ioffe, *Semiconductor Thermoelements and Thermoelectric Cooling,* INFOSEARCH, Limited, London, 1957.

C. F. Kooi, et al., "Theory of the Longitudinally Isothermal Ettinghausen Cooler," *J. of Applied Physics*, v. 34, n. 6, pp. 1735-42, January, 1963.

J. Lukacs, "Semiconductors for Thermal-Electric Generators," *Elektrotechnika*, v. 50, p. 21, 1957.

J. P. Osterle and S. W. Angrist, "On the Choice of Coordinates Used to Describe Thermoelectric and Thermomagnetic Generators," *Journal of Applied Mechanics*, p. 426, September, 1963.

D. E. Smith, et al., "Magnetoelectric and Galvanomagnetic Effects in Bismuth at 80°K," Unpublished, Bell Telephone Laboratories, Inc., Murray Hill, N. J.

R. Wolfe, G. Smith and S. E. Haszko, "Negative Thermoelectric Figures of Merit in a Magnetic Field," *App. Physics Letters*, v. 2, n. 8, pp. 157-159, April 15, 1963.

Raymond Wolfe and George E. Smith, "Semimetals and Thermoelectric Materials," *Semiconductor Products*, p. 29, April, 1963.

Raymond Wolfe, "The Physics of Thermoelectricity," *Semiconductor Products*, p. 23, April, 1963.

D. A. Wright, "Theory of the Nernst-Ettinghausen Generator," *British Journal of Applied Physics*, v. 13, p. 583, 1962.

VITA

Donald Beatty Wall was born in Shelby, North Carolina on April 11, 1934. He is the elder son of Mr. and Mrs. W. H. Wall, Jr. On July 3, 1960 he married Etta Carrine Richbourg from Summerton, South Carolina. They have one son, Donald Beatty Wall, Jr.

Mr. Wall attended public schools in Columbia, South Carolina and graduated from Eau Claire High School in 1952. That year he enlisted in the United States Air Force and served four years. After completing his military obligation he enrolled in the Engineering College at the University of South Carolina. He received the Bachelor of Science Degree in Mechanical Engineering in 1960 and the Master of Science degree in 1962. Mr. Wall's masters thesis is entitled "Determining the Edge Heat Losses in a Guarded Hot Plate Apparatus."

Mr. Wall received a National Science Foundation Fellowship in 1961 and the Ford Foundation Fellowship for 1962-1965. He was elected to Tau Beta Pi and subsequently to associate membership in Sigma Xi.

Mr. Wall enrolled in the doctoral program at Georgia Institute of Technology in the Fall of 1962.